MEASUREMENT OF THE ACOUSTIC FIELD OF RADIATING

CIRCULAR AND RECTANGULAR APERTURES AND

A SCATTERING CIRCULAR DISK

By

CLIFFORD WESLEY MILLER, JR.

Bachelor of Science

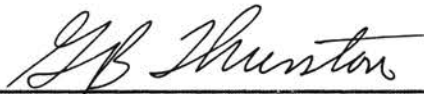Panhandle Agricultural and Mechanical College

Goodwell, Oklahoma

1956

Submitted to the faculty of the Graduate School of
the Oklahoma State University
in partial fulfillment of the requirements
for the degree of
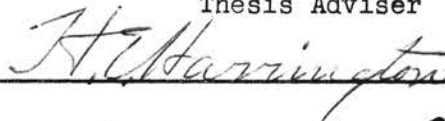MASTER OF SCIENCE
August, 1961

MEASUREMENT OF THE ACOUSTIC FIELD OF RADIATING

CIRCULAR AND RECTANGULAR APERTURES AND

A SCATTERING CIRCULAR DISK

Thesis Approved:

_____
Thesis Adviser

_____

_____
Dean of the Graduate School

PREFACE

The experimental techniques and apparatus used for the measurement of diffracted sound fields have been discussed in this paper. The results of experimental measurements are then compared to elementary diffraction theory, by means of curves obtained from the experimental data.

TABLE OF CONTENTS

LIST OF FIGURES

LIST OF FIGURES (con't.)

LIST OF FIGURES (con't.)

CHAPTER I

INTRODUCTION

During the past 30 years considerable attention has been paid to
the experimental and theoretical study of diffraction by circular disks
and transmission through circular apertures. Most of the experimental
work has been concerned with measurement of the magnitude of the field
variables only, without particular regard to phase factors.

Attempts to obtain mathematically exact solutions of these dif-
fraction problems go back to Rayleigh[1] who succeeded in evaluating the
case of transmission through a hole which has dimensions very small in
comparison with the wave length. Only recently have Bouwkamp[2], Spence[3],
and Wergeland and Storruste[4] independently reported solutions for the
case of a circular aperture which is valid over a large frequency
range.

In this work a method of making field measurements, before the
reverberations due to multiple reflections are built up in the region
of measurement, has been presented. Limitations of the method as re-
lated to the specific laboratory environment are pointed out. Mea-
sured field conditions along the axis, along the lateral surface, and
at fixed radial distances, for the circular aperture have been com-
pared to elementary diffraction theories for three cases: (1) $D/\lambda > 1$
(2) $D/\lambda \approx 1$ and (3) $D/\lambda < 1$ where D is the diameter of the
aperture and λ the wave length. Also, the measured pressure fields

of a rectangular aperture and a circular disk have been compared to the respective theories.

The purpose of this work was to obtain more complete information on the properties of the acoustic field than is normally available. Thus the field measurement includes not only pressure magnitude determinations but also the phase of the pressure and the magnitude and phase of the pressure gradient. This more detailed structure of the acoustic field is then compared with the properties predicted by elementary theoretical concepts. In order to perform these measurements it was necessary to use conventional pulse techniques, but to improve the details of the handling of the pulses in order to carry out the required phase measurements.

The experimental results show good agreement with those predicted by elementary theories, where it is expected that these theories should apply.

CHAPTER II

TECHNIQUES OF MEASUREMENT

A. <u>General Background</u>

Consider the sound field originating from a source in a room. If reflection from the walls of the room could be eliminated the sound field would be the same as the field of the source in free space.

The effect of the room can be eliminated if the measurements can be made before the reverberation become effective, or by enclosing the experimental equipment in a room with non-reflecting wall so that all the sound incident on the walls is absorbed.

For the measurements presented herein, a pulse technique was used so that measurements of the field could be made before the reverberations became effective. The time between pulses was such that the reverberations in the room due to the previous pulse decayed to a level such that they were undectable before the next pulse began. The reverberation time can be decreased by lining the walls with an acoustic absorbant material.

B. <u>Pulse Technique of Measurement</u>

With the horn mounted to the rear of the anechoic chamber used in this work it takes approximately six milliseconds, from the time the electrical pulse is fed to the horn, for the sound pulse to reach the front of the chamber. As the microphone is moved out in the field away

3

from the chamber this delay time is increased at a rate of approximately 3.3 miliseconds per meter. Because of this inherent delay, it was necessary to use the delay trigger circuit so that a more efficient use of the oscilloscope trace could be made. Since the oscilloscopes are triggered with the gate drive, without the delay trigger the six or more milliseconds of sweep during the delay were of no value. With the delay trigger the beginning of the sound pulse can be shifted to the beginning of the sweep, by adjusting the trigger level of the oscillo-scopes. Likewise, the trail off of the pulse can be observed by changing the sign of the triggering mode.

A simulated signal equal in magnitude and phase to the acceptable portion of the pulse was constructed visually on a dual beam oscillo-graph. The pressure and phase measurements were then made from this simulated signal.

The gating circuit can be driven by any of the three wave forms from the function generator: (1) sine, (2) square or (3) triangular waves. Illustrations of the three driving modes are discussed in the next section.

C. Nature of the Sound Pulses

The following photographs were taken from the 533 oscilloscope using a model 196-A Polaroid Land camera. For all the photographs shown a 4 x 4 foot aluminium plate was suspended at the end of the room to reflect more of the sound such that the effects of the reflected waves would be enhanced. The microphone is approximately 50 cm. from the front of the chamber.

The time represented between the dial calibration is 10 milliseconds.

The pulse begins as the sound wave train reaches the microphone from the aperture in the front of the chamber.

Figures 1 and 2(a) show the acoustic pulse at different points on the axis of the circular aperture, using the square wave as the gating drive.

Note that between 9 and 16 milliseconds a definite transient appears at the beginning of the pulses. This transient is present when the square wave drive is used and is the result of the signal and the gate drive not being synchronized. If the signal starts at zero amplitude each time the gate opens, this transient does not appear, at least with such magnitude. This can be verified by carefully tuning the two generators.

The sound pulse shown in figure 1(a) will now be discussed briefly. Note that the region between 20 and 35 milliseconds is relatively flat and uniform. This is the region of the primary field from which measurements are made. The peak to peak amplitude of this region is read from the 130-A oscilloscope as described earlier.

The small dip in amplitude shown from 36 to 41 milliseconds, is due to the interference of the wave train reflected from the plate at the wall and the primary wave train. The length of the dip corresponds to the time required for the reflected wave train to travel from the microphone to the front of the chamber and back to the microphone. At the front surface of the chamber this dip is not visible and the width of the dip increases as the microphone is moved away from the chamber. The remaining 50 milliseconds of the pulse correspond to the field due to the presence of the three waves: primary wave, wave reflected from the plate at the wall, and the doubly reflected wave from the face of
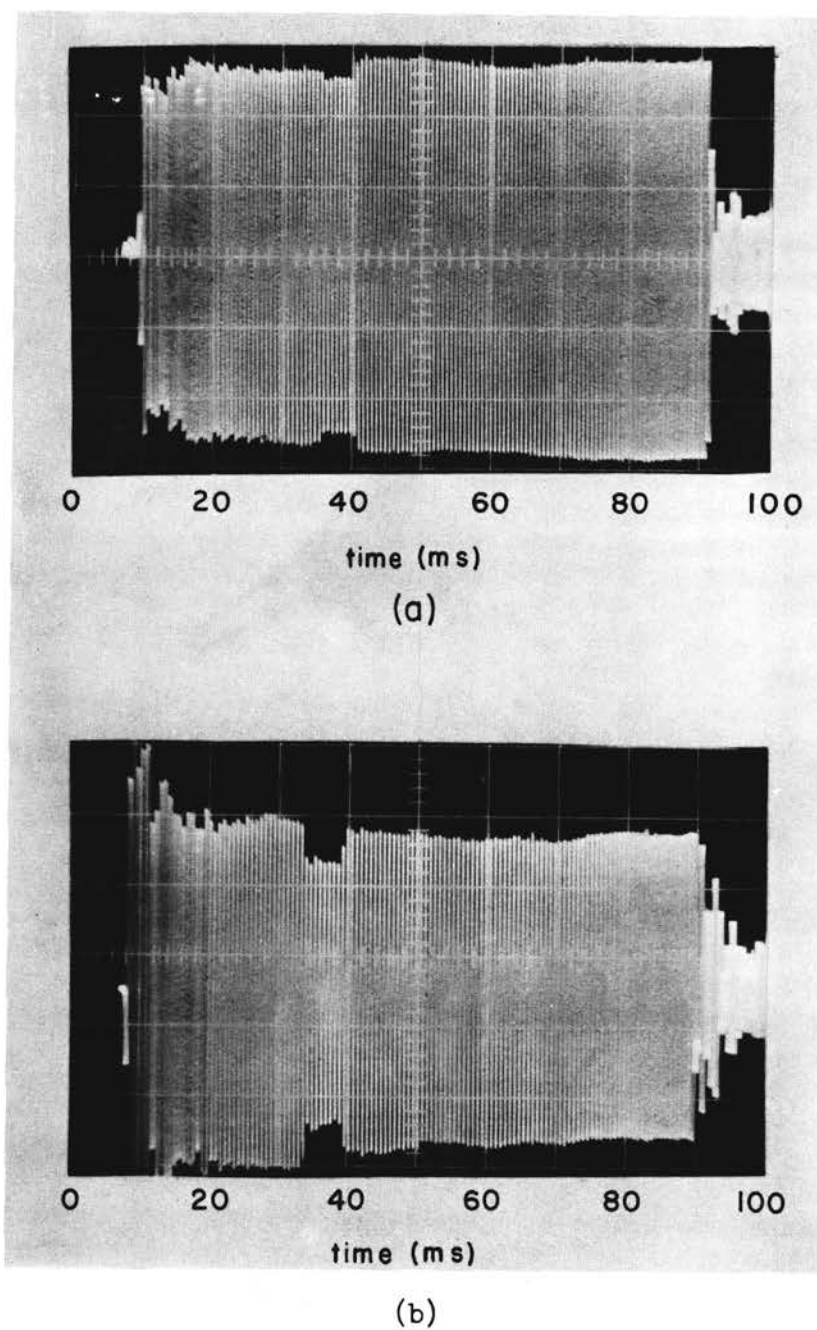
Figure 1

(a) Acoustic pulse 50 cm from aperture
with square wave drive

(b) Acoustic pulse 53 cm from aperture
with square wave drive

time (ms)

(a)

time (ms)

(b)
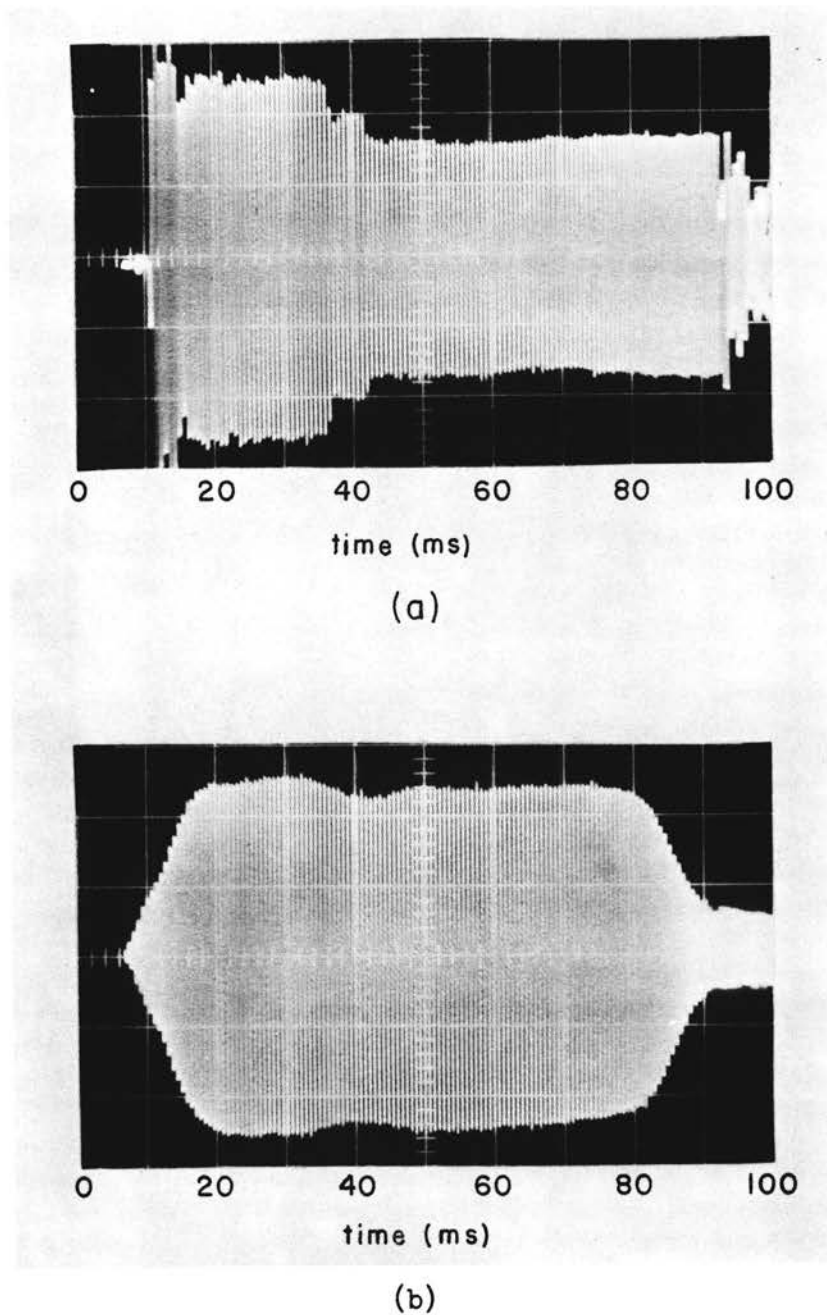
Figure 2

(a) Acoustic pulse 47 cm from aperture
with square wave drive

(b) Acoustic pulse 50 cm from aperture
with triangular wave drive
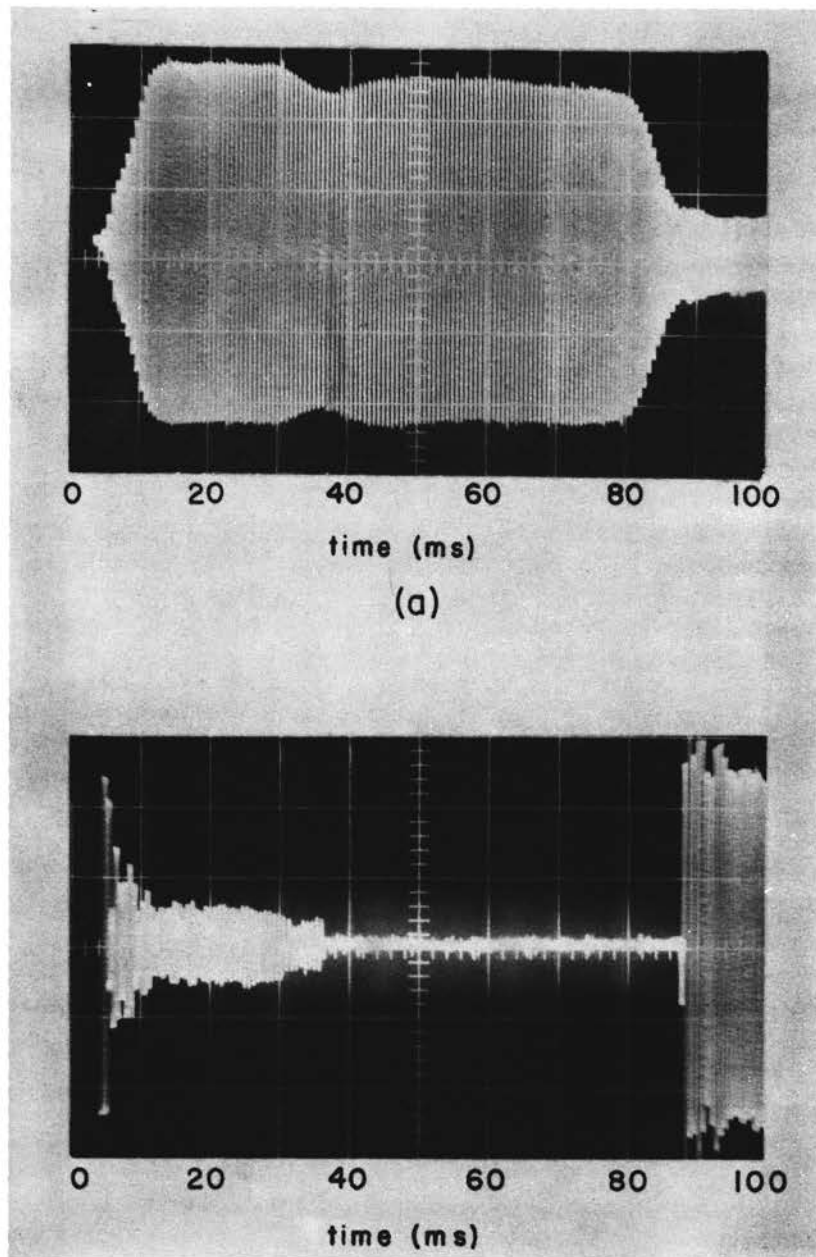
Figure 3

(a) Acoustic pulse 50 cm from aperture
with sine wave drive

(b) Trail off and dead time 50 cm from
aperture with square wave drive
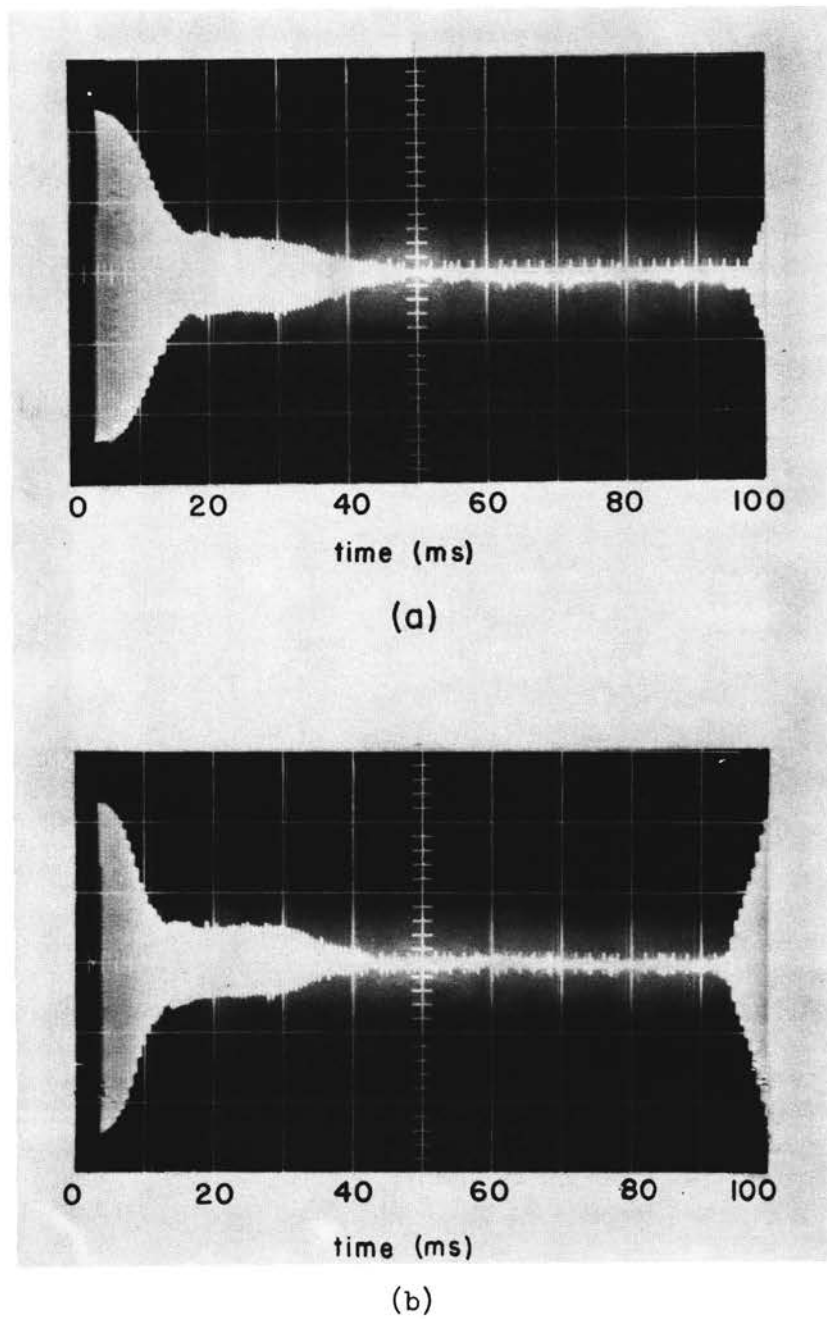
Figure 4

(a) Trail off and dead time 50 cm from
    aperture with triangular wave drive

(b) Trail off and dead time 50 cm from
    aperture with sine wave drive

the chamber.

Figures 1(b) and 2(a) reveal essentially the same information as does figure 1(a). However, for these two figures, a 4 x 4 foot plate was placed along one side wall, approximately even with the chamber and orientated in such a way as to greatly enhance the side reflections. Because the plate had to be so near the chamber and microphone, and because the orientation is critical for enhancement of the reflection, the reflections from the walls and were neglected in the measurements taken. The position of the microphone in figure 2(a) is such as to show the destructive interference of the three waves.

Figures 2(b) and 3(a) show the same pulse as figure 1(a), except the gate drive is the triangular and sine wave respectively. Note the gradual build up of the two pulses and the beginning transient does not occur as with the square wave drive, because the amplitudes of the first few cycles are small. However, for the measurements taken, the square wave drive was chosen because the sharp definition makes possible definite identification of envelope characteristics. At certain points in the field it could be possible, if the sine of triangular wave drives were used, to make measurements on the modified field unrealized by the operator. It is felt, however, that with the sharp definition by the square wave drive this error could be eliminated.

Figures 3(b) and 4 show the trail off and the dead time of the square, triangular and sine wave drives respectively. In figure 3(b) from 5 to 9 milliseconds, the same type transient appears as at the beginning of the pulse as seen at 90 milliseconds and in figure 1(a). From 10 to 30 milliseconds there is the interference of the two reflected wave trains then from 30 to 36 milliseconds the end of the wave train

reflected from the front of the chamber. It is evident that the rever-
beration time of the room is short even with the reflecting plate be-
cause no other identifiable signal appears during the remainder of the
dead time. Thus the initial condition of quietness in the room is almost
reached before the next pulse arrives. Also, in figure 3(b) the first
13 milliseconds of the beginning of the next pulse can be seen. The
larger transient than in figure 1(a) is due to the signal starting at a
greater amplitude when the gate was opened.

CHAPTER III

INSTRUMENTS AND EQUIPMENT

A. Basic Equipment

The measurements described herein were made in the semianechoic
room of the Acoustics Laboratory. The dimensions of the room are
approximately 35 x 16 x 8 feet. The walls and ceiling of the room are
lined with a $1\frac{1}{2}$ inch layer of pressed fiberglass, which has its outer
surface painted. The floor is covered with cork tile.

The experimental equipment consists basically of: (1) electronic
equipment, (2) anechoic chamber, and (3) metal supporting frame. The
arrangement of the equipment in the room is illustrated in figure 5.

B. Steel Supporting Frame

The metal supporting frame is a five-inch-steel "I" beam supported
on coasters by two pieces of two-inch steel pipe. In the center of the
"I" beam is attached a thrust assembly on which is mounted an angle
vernier. The thrust assembly has attachments, which will support the
4 x 4 foot plates, or the microphone.

The microphone is supported by a $\frac{1}{2}$ inch steel rod, attached to the
thrust assembly, such that it can easily be moved for axial measure-
ments and also held rigidly for radial measurements. The frame can
be seen in figure 5.

FIGURE LEGEND

Figure 5   Experimental Equipment

      (A) hp 202-A function generator
      (B) hp 202-B low frequency generator
      (C) hp 450-A amplifier
      (D) McIntosh MC-30 amplifier
      (E) hp 130-A oscilloscope
      (F) Tektronix 533 oscilloscope
      (G) ITECO 200-AB phase meter
      (H) Gate, phase shifter and trigger
      (I) Meter stick for lateral positioning
          of microphone
      (J) Thrust assembly and angle vernier
      (K) Circular aperture in face of chamber
      (L) Source, P-30 University horn
      (M) Microphone and preamplifier
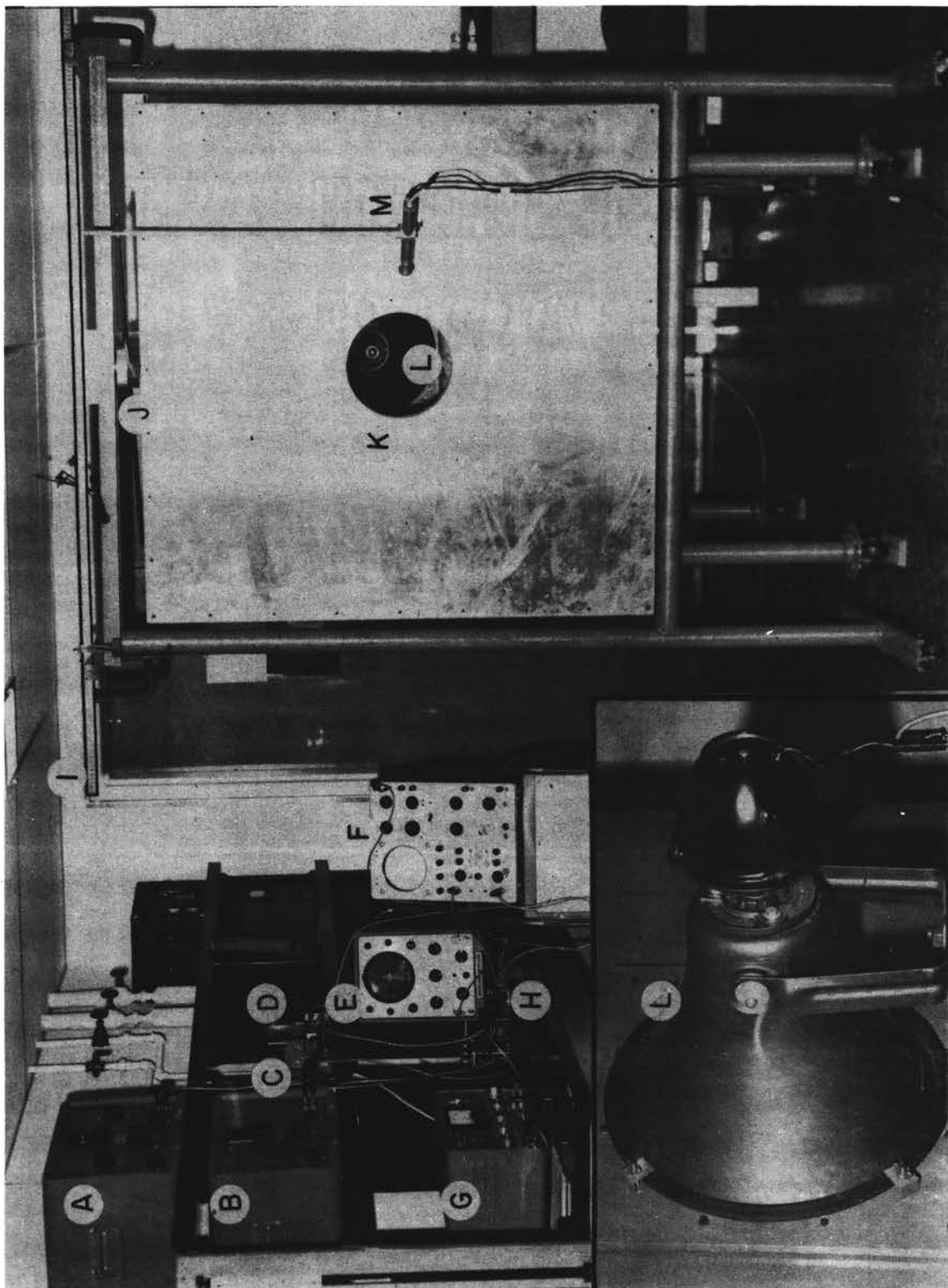
Figure 5

C. Anechoic Chamber

The anechoic chamber is supported on coasters by four two-foot lengths of two-inch steel pipe. The outside dimensions of the chamber are 4 x 4 x 4 feet. These dimensions were chosen because they are the largest dimensions which would allow transport of the chamber from the shop to the laboratory and also allow for the most efficient use of materials. The walls of the chamber are made of 3/4 inch plywood and the inside was lined with two layers of two-inch fiberglass mats of different density, the layer next to the plywood being the more dense. One side of the chamber (hereafter called the front) is open so that different interface materials may be attached.

In the center of the rear face (the face opposite the open front) was cut a square opening 15 x 15 inches, to which was mounted the P-30 University horn.

For this work the front of the chamber was closed with a 4 x 4 foot aluminium plate $\frac{1}{4}$ inch thick. Two layers of the fiberglass, used on the walls and ceiling of the room, were glued by contact cement, to the inside of the plate to reduce internal reflections from the plate and to damp any flexural waves set up in the plate by the incident sound waves.

A window 10 inches in diameter was made in the center of the plate. This diameter was chosen so that the diameter would be small and large compared to the wave length of the sound within the frequency range of the horn. To this window can be attached, by means of mounting rings, many variations of the aperture, such as rectangular apertures, membranes, etc.. The microphones and samples used in this work

are shown in figures 6, 7, 8 and 9.

D. Electronic Equipment

The electronic equipment consists of:

1 P-30 University horn

1 MC-30 McIntosh power amplifier

1 450-A Hewlett Packard fixed gain voltage amplifier

1 202-A Hewlett Packard function generator

1 202-B Hewlett Packard low frequency generator

1 130-A Hewlett Packard single beam oscilloscope

1 533 Tektronix dualbeam oscilloscope with type CA plug in unit

1 200-AB ITECO Phazor phase meter

1 16-PI Power supply

1 P-16 Preamplifier with Kellogg capacitance microphone

1 R-C delay trigger circuit

1 Transistor gating circuit

1 Phase shifting network

E. R-C Delay Trigger

The R-C delay trigger circuit was a simple series R-C network.
The output of the 202-A function generator was fed to the input of the
trigger, then the voltage across the capacitor was fed to the external
trigger of the two oscilloscopes. Using this delay trigger one could
observe the entire gated burst of signal (hereafter called the pulse),
the entire dead time, the beginning of the pulse and the trail off of
the pulse, simply by changing the triggering level of the oscilloscopes.

FIGURE LEGENDS

Figure 6 Microphone, preamplifier, and circular aperture

Figure 7 Gradient microphone
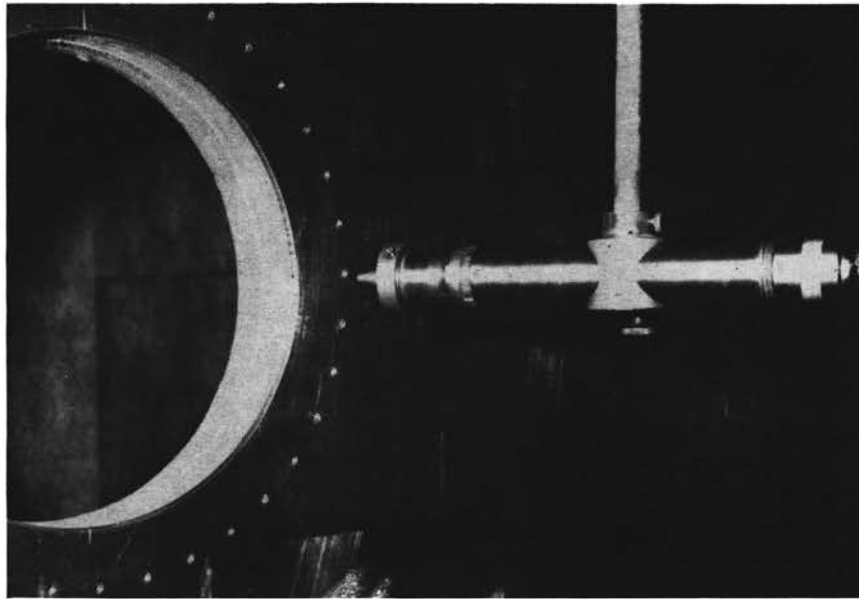
Figure 6
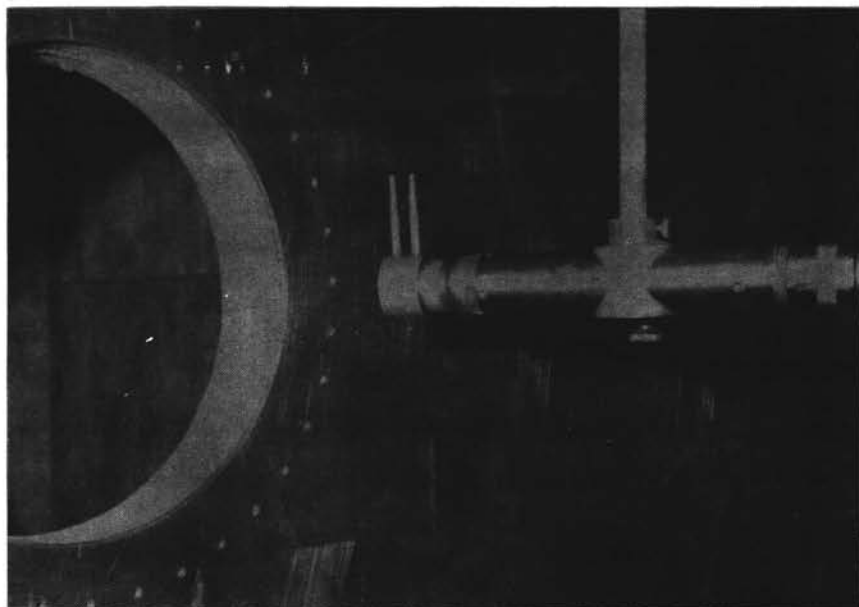
Figure 7

FIGURE LEGENDS

Figure 8 Rectangular aperture, mounting rings

Figure 9 Circular disk 1.5 m. from aperture
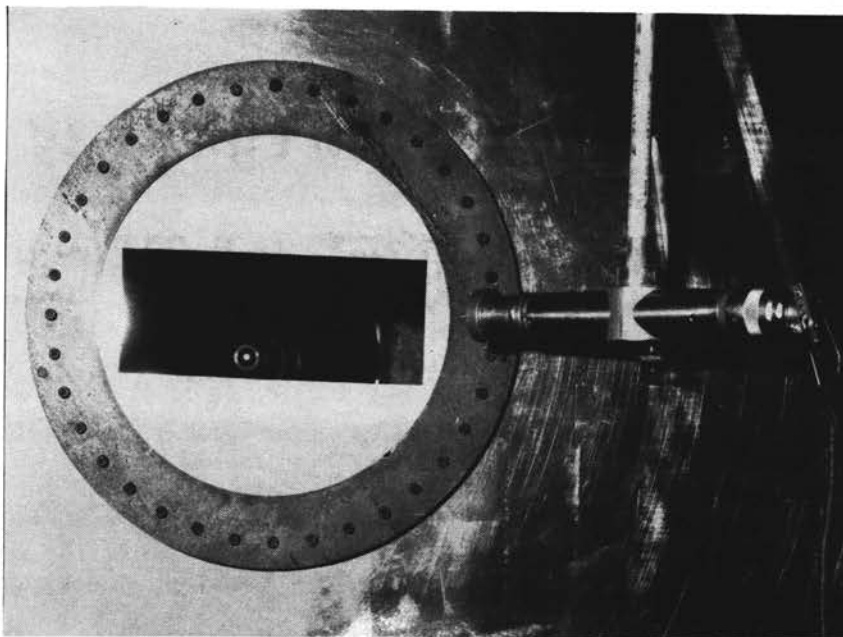
Figure 8
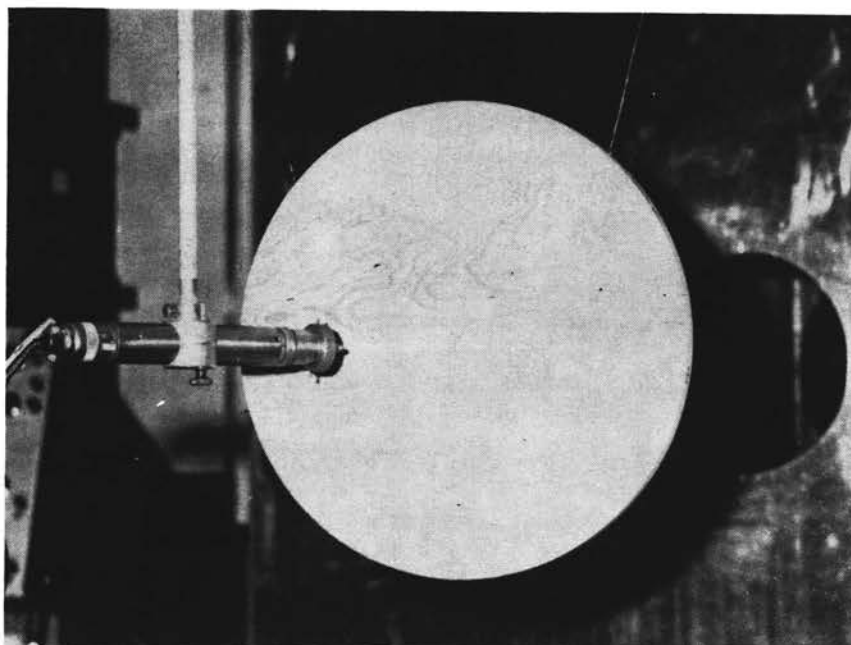
Figure 9

F. <u>Transistor Gating Circuit</u>

The gating circuit[5] was a 2N78 transistor operating in its switching mode and used as a switch. Figure 10 shows the gating circuit in which the transistor is effectively shunted across the signal path.

The 1 k ohm resistor R in the collector circuit and the input impedence of the McIntosh power amplifier Z effectively make a voltage divider from point A. When the transistor is in its "off" mode, a voltage applied at point A will appear across Z decreased by the ratio of R to R $\neq$ Z. The "off" mode occurs when a positive d-c voltage is applied to the base of the transistor.

With a negative d-c voltage applied to the base the transistor is biased "on." The negative voltage is chosen such that the transistor is in its saturation state, with the result that it will shunt a very low impedence from point C to ground. While the transistor is in this mode, any signal at point A will be dropped across R and none (or very little) will appear across the output terminals.

Thus by using the function generator as the base drive the base can be biased alternately positive and negative, producing pulses of the signal applied to point A. The diode allows a positive base voltage such that the transistor is "off" and still a large biasing signal can be used such that the negative voltage will drive the transistor to saturation rapidly.

The length of the gated pulse is controlled by the frequency of the base biasing signal. There are two inherent disadvantages in the gate: (1) the dead time, by nature of the symmetry of the biasing signal, is the same length as the pulse, and (2) there is no sychro-
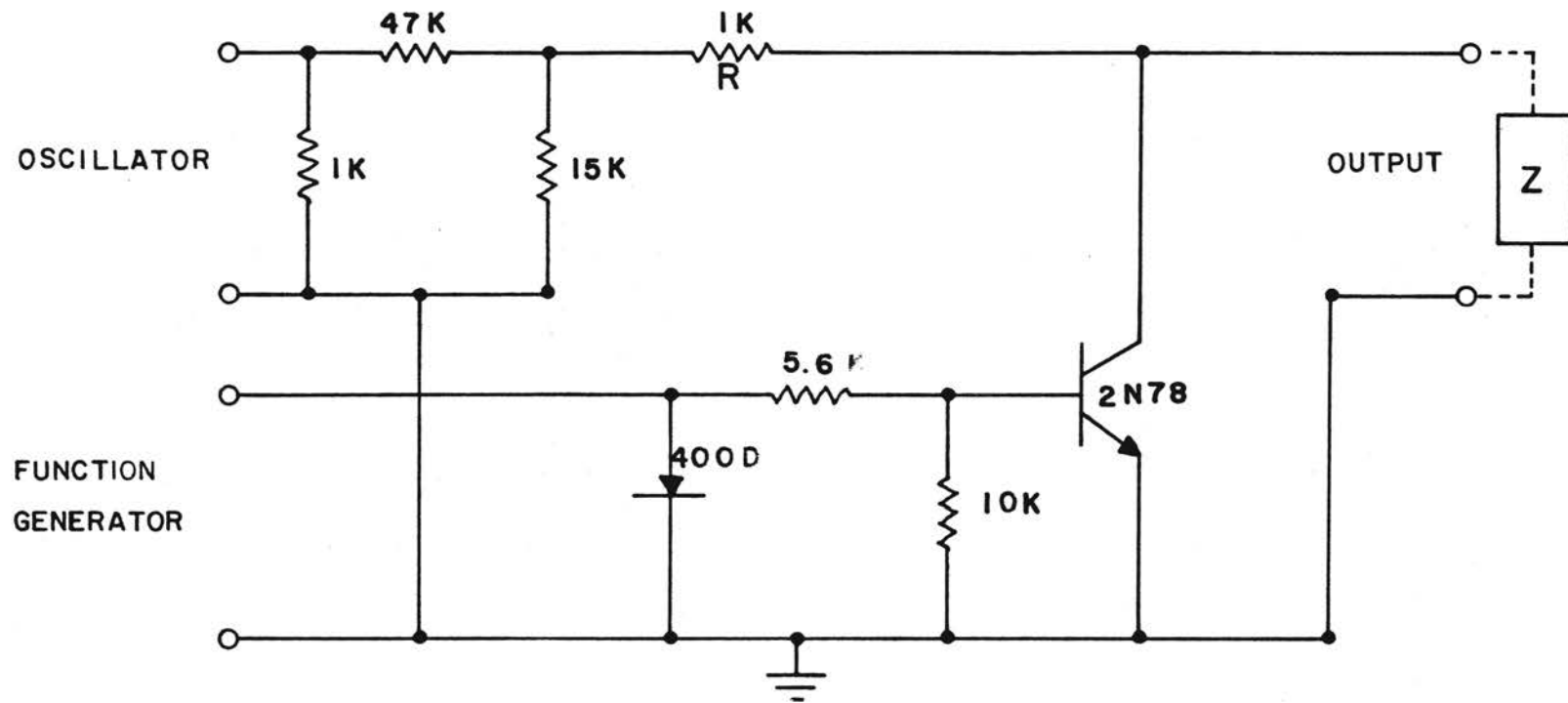
Figure 10. Gating circuit

nization between the signal of the pulse and the biasing signal. As a result of the latter, the starting point of the gated signal cannot be controlled.

G. Phase Shifting Circuit

The phase shifter shown in figure 11 is a basic phase shifting network. The .001 mfd capacitor was put in the circuit to provide a fixed shift in the output. Without this capacitor the total quadrature cannot be covered continuously by the network.

The double pole double throw switch S_2 makes possible an instantaneous phase shift of 180°. The transformer serves only to isolate the ground points of the two sides of the network.

H. Experimental Arrangement

A block diagram of the experimental equipment is shown in figure 12. The output of the 202-A was used to drive the gate and through the trigger delay to externally trigger the two oscilloscopes. The output of the 202-B was gated by the gate circuit, amplified by the McIntosh power amplifier and fed to the University horn. Also, the output of the 202-B was used as a reference signal for the phase determinations.

The output signal of the microphone was fed to the fixed gain (40db or 20db) 450-A voltage amplifier then to the vertical input of the 130-A oscilloscope and to channel A of the Tektronix 533 oscilloscope. The peak to peak amplitude of the output signal from the microphone was read directly from the calabrated 130-A oscilloscope.

Since the phase meter can be used only on continuous signals, the

reference phase signal was fed through the phase shifter network to channel B of the 533, and was shifted until it was in phase with the output signal of the microphone. The relative phase between the shifted reference and the fixed reference was then read from the phase meter.
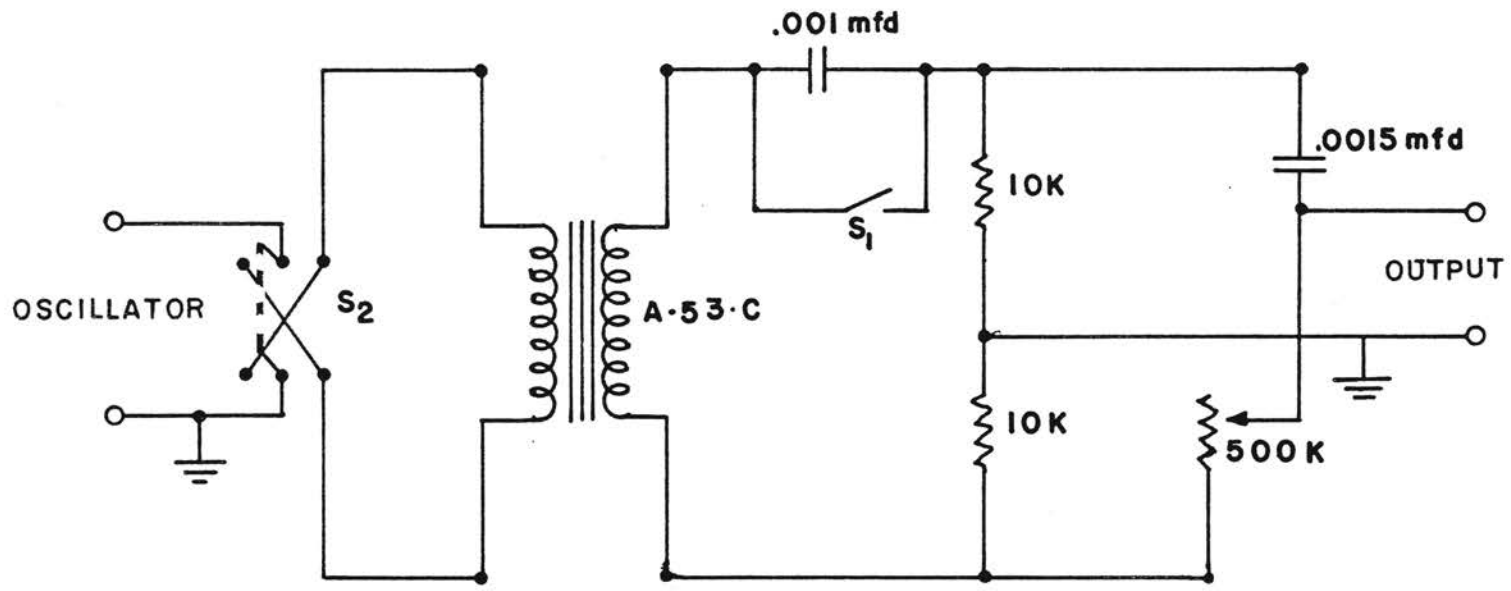
Figure 11. Phase shifting circuit
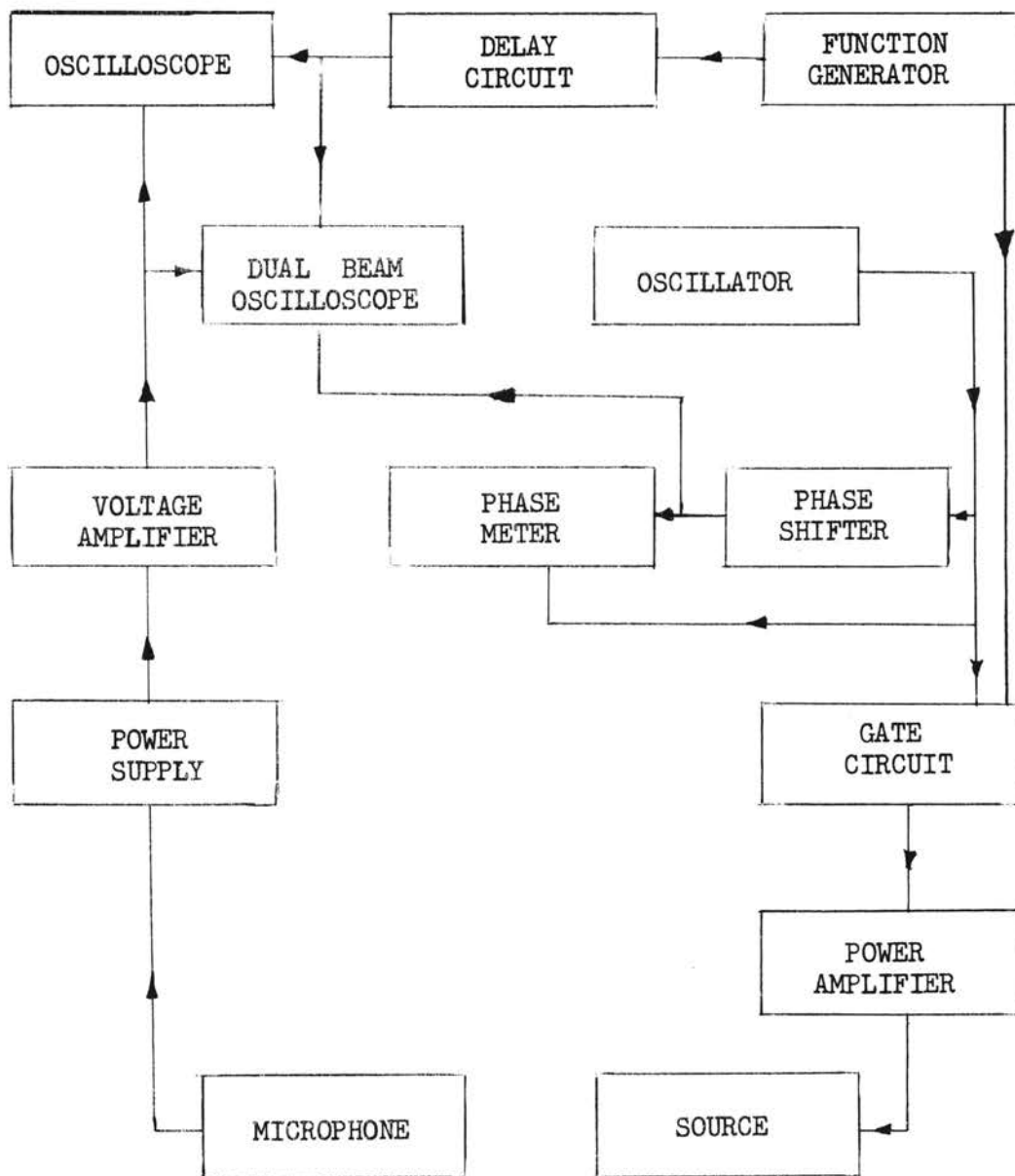
FIGURE 2

Block diagram of experimental equipment.

CHAPTER IV

CIRCULAR APERTURE

A. The Radial Pressure Field

The angular direction, from the normal to the aperture, of the maximum and minimum pressures may be calculated from the Fraunhofer diffraction theory.[6,7]

If β is the angle measured from the normal to the direction of the maximum or minimum, the values of the angle β are given by

$$SIN \ \beta = n' \ \frac{\lambda}{D} \tag{1}$$

where λ is the wavelength of the incident wave, D , the diameter of the aperture and n' , a number computed for each successive maximum or minimum from the function[8]

$$P = P_o \left[\frac{2 \ J_1(x)}{x} \right]^2 \tag{2}$$

where $x = n' \pi$. The pressure maxima occur when $J_1(x)$ is maximum and minima occur when $J_1(x)$ is zero.

The first four maxima occur when n' has the values of 0, 1.635, 2.679 and 3.699 respectively. Similarly, the first four minima occur when n' has the values of 1.220, 2.233, 3.238 and 4.250 respectively.

From equation (1) we see that the value of β for a particular n' depends on the ratio λ/D . When $\lambda/D > 1$ there will be no

minima and the aperture will radiate as a point source. When $\lambda/D = 1$ there will be a minima in the region of $\beta = 90°$ and when $\lambda/D < 1$ the minimum points will appear according to equation (1).

These three conditions are approximately satisfied using the aperture 25 cm. in diameter with frequencies as follows:

Case 1 -- 500 cycles per second

Case 2 -- 1500 cycles per second

Case 3 -- 8000 cycles per second

The velocity of sound in air for an atmospheric pressure of 73.7 cm., which is the average pressure in the laboratory, is 33,960 cm./sec. Using this value for the velocity of propagation we have:

Case 1 $\lambda = 79.1$ cm.

Case 2 $\lambda = 26.4$ cm.

Case 3 $\lambda = 4.95$ cm.

We shall now look at the three cases separately.

Case 1:

The ratio of λ/D is less than 1; thus, the radial pressure field will appear as concentric half circles with center at the center of the aperture.

Case 2:

The ratio of λ/D is of the order of 1; thus, the radial pressure field will appear as a single lobe, with decreasing pressure as the angle β approaches 90 degrees. This case will be discussed in more detail later.

Case 3:

Using equation (2) the calculated values of n' for the four

minima are

$$n' = 1.22, 2.23, 3.34 \text{ and } 4.25.$$

The corresponding values of β as obtained from equation (1) are

$$\beta = 13.95°, 26.15°, 41.45° \text{ and } 62.6°.$$

Using equation (2) we can compute n' for which maxima will occur. The values of n' for the first four maxima are

$$n' = 0, 1.635, 2.679 \text{ and } 3.699.$$

The corresponding values of β are

$$\beta = 0°, 18.9°, 32.0° \text{ and } 47.2°.$$

Figure 13 is a polar graph of the observed radial pressure field for case 3 at distances of 30 and 200 cm. The minimum and maximum points correspond well to the values given by the Fraunhofer diffraction theory above.

Figure 14 shows a polar graph of the radial pressure field as observed at 15, 32, 50 and 85 cm. for case 1. From figure 14 we note that the near field produces an almost spherical wave whereas at greater distances the wave deviates from the spherical form. This deviation is due primarily to reflections from the side walls, floor and ceiling of the room.

The magnitude measurements are accurate to within ± 1 db, and the relative phase accurate to within ± 5 degrees, based on the reproducability of the data. The positions relative to each other are within ±0.5 mm, and the exact positions relative to the center of the aperture are accurate to within 2 mm. For some of the curves contained herein, a simple straight line connection between data points is used because there is insufficient data to more completely define the field. However, when smooth curves are used, these curves lie within the error

mentioned above except where otherwise indicated.

The error in pressure and phase is due basically to (1) position of microphone, (2) the presence of the microphone, supports, etc., in the field, (3) meter and oscilloscope reading and (4) transmission through the front of the chamber as shown in Appendix I.

The error in position is due to (1) assuming the microphone hangs vertical at each position, since it is free to swing as a pendulum, (2) fluctuations in the calibrations of the meter stick and (3) the position setting on the meter stick.

B. The Axial Pressure Field

The Fresnel diffraction theory[7] can be used to determine the pressure field along the axis of a circular aperture if we assume that the incident wave is nearly plane. This condition is approximated in the experimental arrangement.

How does the pressure of the axial field change as the point of observation moves along the axis? The radii of the Fresnel zones depend on the position of observation. Thus we find the pressure goes through a series of maxima and minima, occurring respectively when the aperture includes an odd or even number of Fresnel zones.

The outer radii of the Fresnel zones are given by

$$r_n^2 = n \left[x\lambda + \left(\frac{\lambda}{2}\right)^2 \right] \tag{3}$$

where r_n is the outer radius of the $n\,th$ zone, n an integer, x the distance from the aperture to the point of observation on the axis, and λ the wave length of the wave.
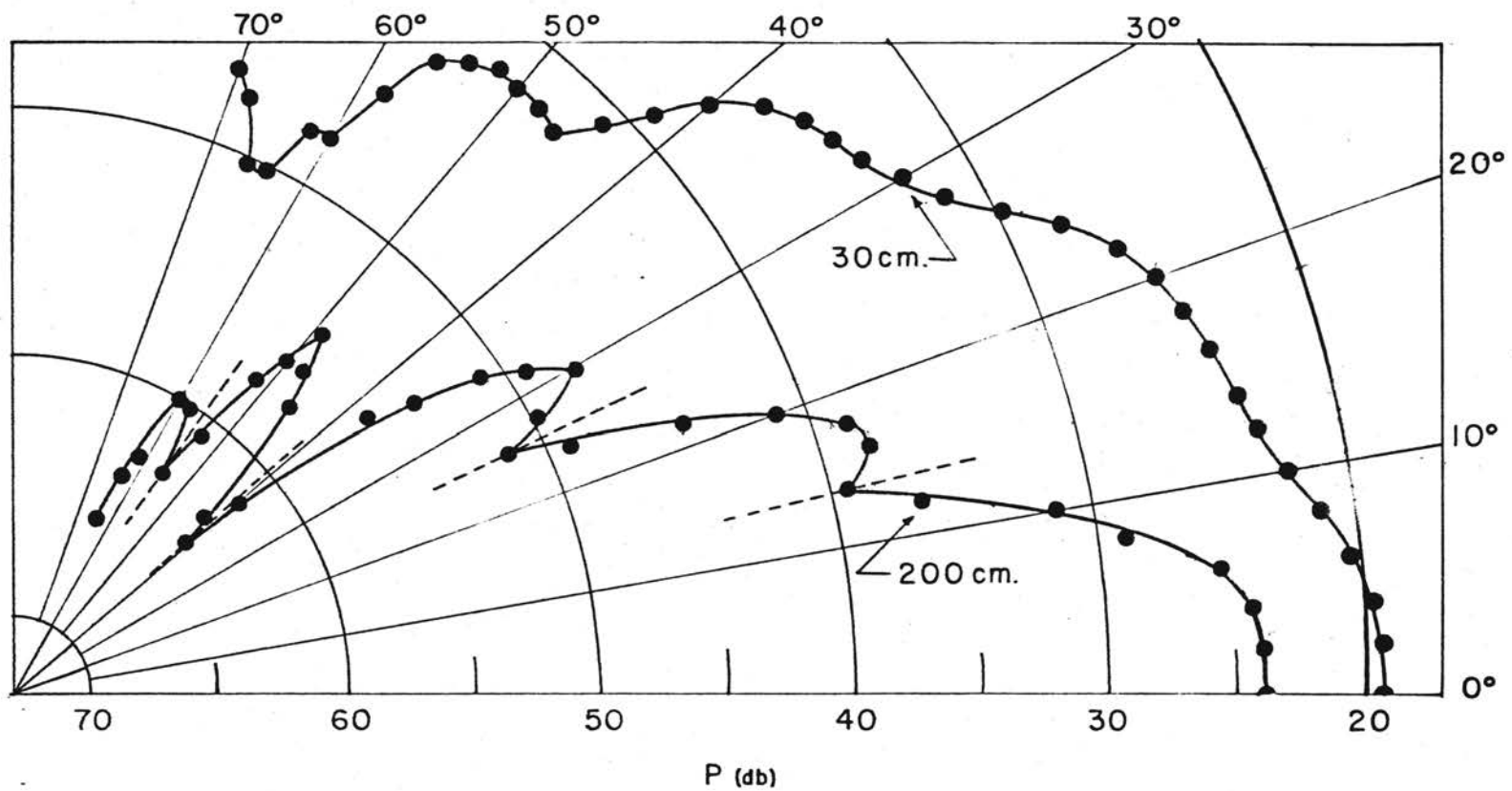
Figure 13. Pressure vs. azimuthal angle, circular aperture, f = 6000 cps. (See Appendix II for pressure reference level.)
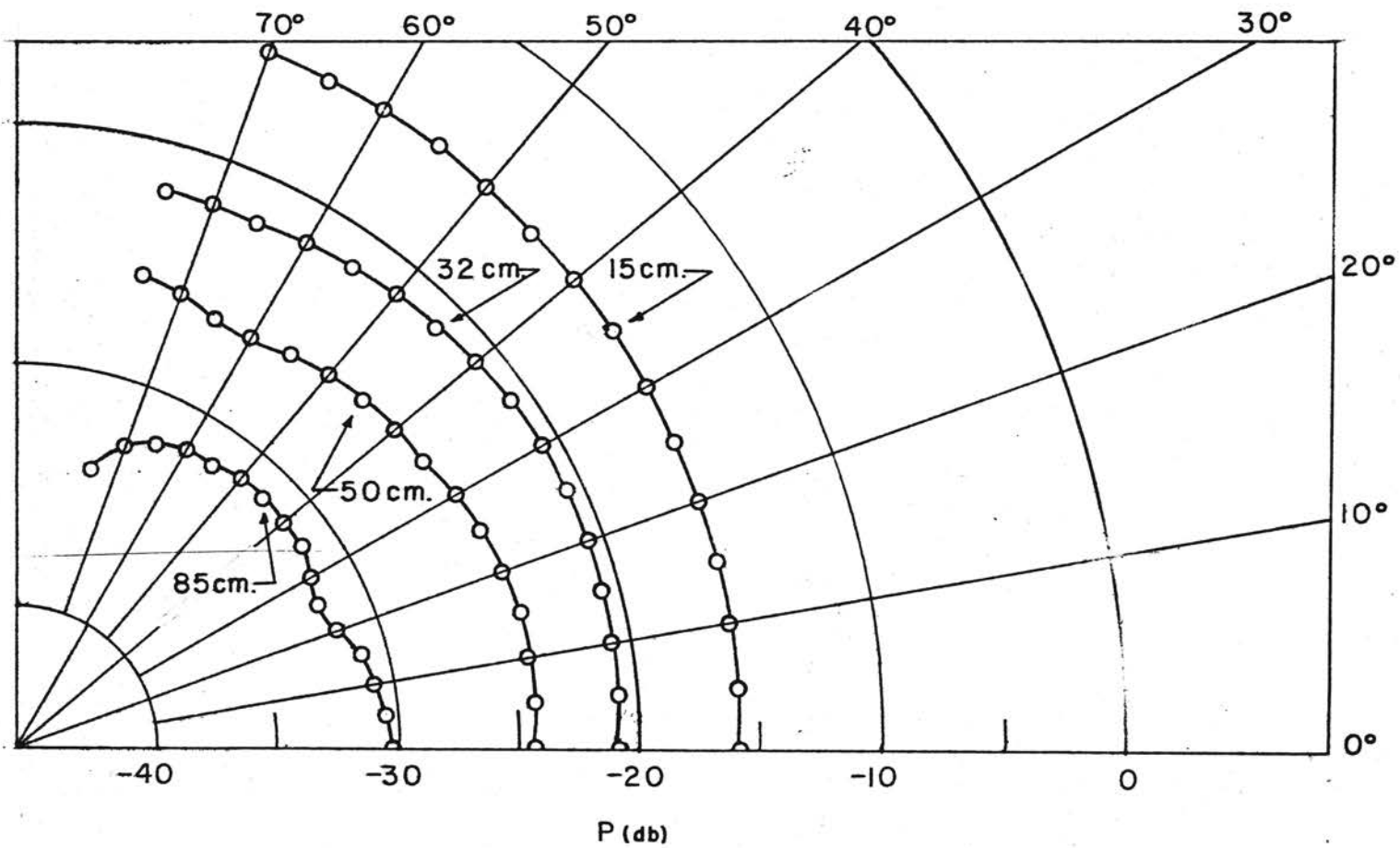
Figure 14. Pressure vs. azimuthal angle, circular aperture, f = 500 cps. (See Appendix II for pressure reference level.)

Considering the vibration spiral, we note that as χ decreased from a distant point the radius r_n of the $n\,th$ Fresnel zone decreases; hence, an increasingly large fraction of the first Fresnel zone appears through the aperture. The pressure therefore increases and reaches a maximum when the radius of the first Fresnel zone is equal to the radius of the aperture. That is, when

$$r_1 = \frac{D}{2} \tag{4}$$

where D is the diameter of the aperture. Thus from equation (3) the distance from the aperture to the maximum points is given by

$$\chi_m = \frac{r_n^2}{n\lambda} - \frac{\lambda}{4} \tag{5}$$

As the point of observation moves closer to the aperture, the maxima and minima follow each other at decreasing distances. When the distance χ is not very large compared to the radius of the aperture, the distances between successive maxima and minima approach the magnitude of the wave length. Under these conditions the maxima and minima can no longer be practically observed.

Case 1:

Since the aperture acts essentially as a point source the wave will propagate out from the aperture as a spherical wave. Thus the diffraction theories of Fraunhofer and Fresnel do not apply.

Figure 15 shows the axial variations of pressure as the point of observation moves away from the source for case 1.

Case 3:

Using equations (3) and (4) we find that as the distance χ is de-

Figure 15. Pressure vs. axial distance, circular aperture, f = 500 cps. (See Appendix II for pressure reference level.)

Figure 16. Pressure vs. axial distance, circular aperture, f = 8000 cps. (See Appendix II for pressure reference level.)

creased the maxima will appear at:
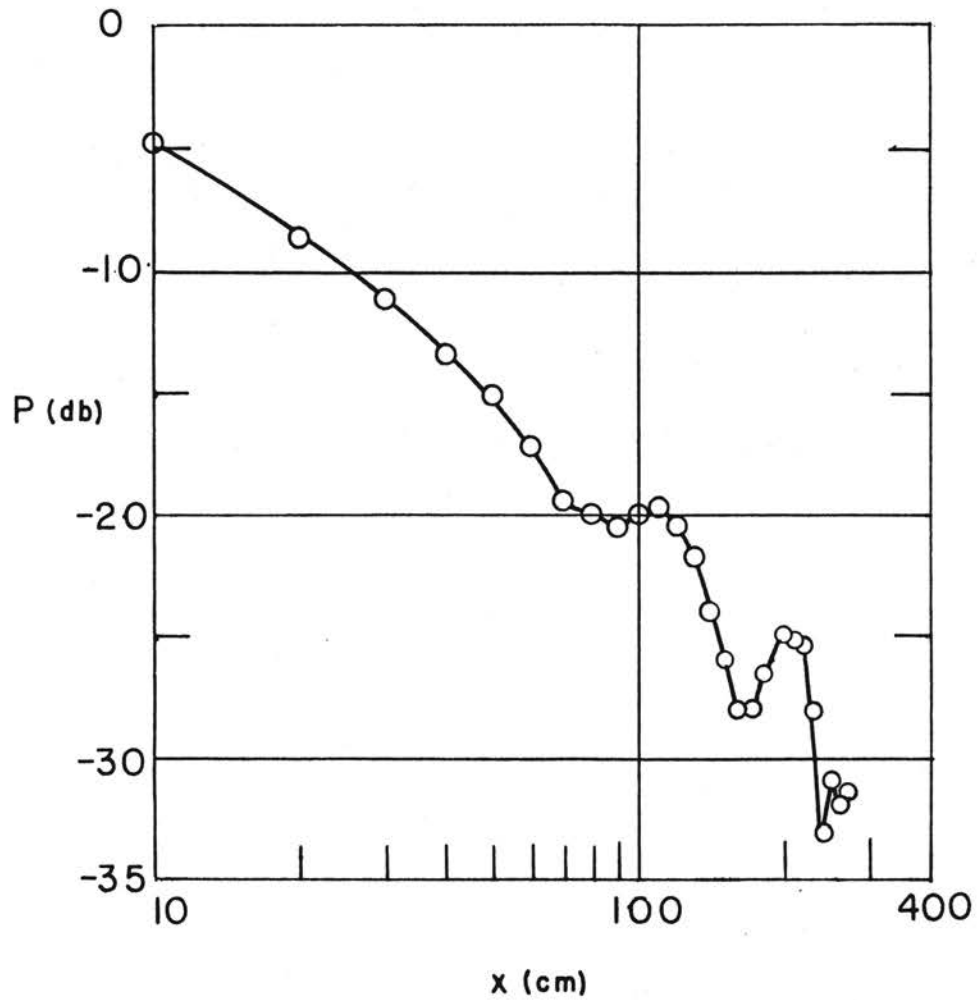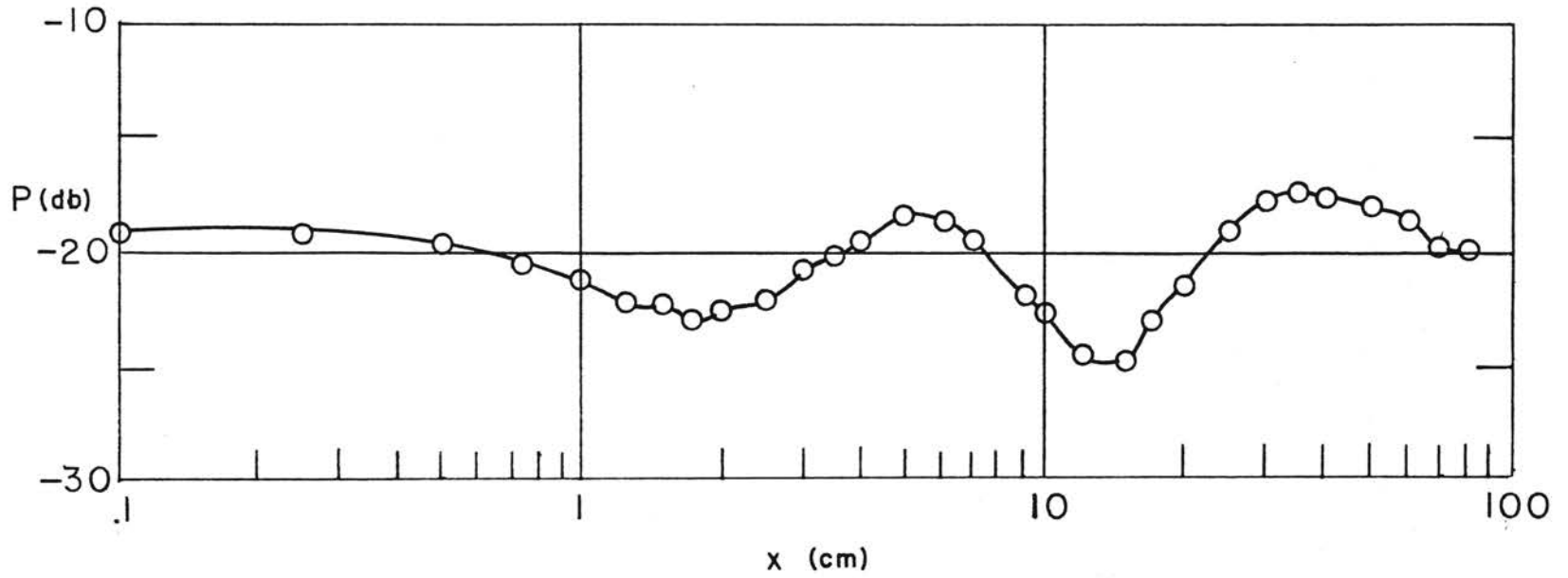
χ = 30, 9.2, 5.0, 3.2, 2.2, 1.6 cm.

The corresponding minima points will appear at:

χ = 14.4, 6.6, 4.0, 2.6, 1.8, 1.02 cm.

Figure 16 shows the axial pressure variations as the distance increases, for case 3. The regions of the two maxima and minima compare favorably with the first two values given above.

C. The Near Field or Lateral Pressure

R. D. Spence[9] has compared the predictions of the Kirchhoff approximations with those of the exact theory for the problem of diffraction by a circular aperture. His conclusions are: (1) The Kirchhoff assumption (constant pressure in the aperture) gives an approximately correct value for the average value of the normal pressure provided the radius of the aperture is nearly equal to or greater than the wavelength; (2) The diffraction pattern calculated from the Kirchhoff approximations are reasonably accurate for angles less than that of the first minimum provided the radius of the aperture is nearly equal to or greater than the wavelength.

The pressure distribution in planes perpendicular to the axis of the aperture has been investigated theoretically and experimentally by G. Bekefi.[10] Within the aperture, he found pressure maxima and minima across the aperture which contridicts the Kirchhoff assumption.

He found that the pressure distribution remained unchanged as long as the ratio of aperture diameter to wavelength was kept constant. Also, he found that the relative pressure variations are greatest when D/λ is half-integral--that is, when $D/\lambda = m + \frac{1}{2}$. Central maxima were

found when m is even and minima when m is odd. He has also modi-
fied the Fresnel-Kirchhoff theory in an attempt to make it valid for
field points near the aperture. This theory compares very favorably
with his experimental results provided the field points are at a dis-
tance from the screen greater than the aperture diameter. At distances
less than this the agreement is poor and becomes progressively worse
as the aperture plane is approached.

This theory of Bekefi indicates that as the observation point moves
toward the geometrical shadow of the aperture from the center along a
diameter, oscillations in the pressure will occur. As the geometrical
shadow is crossed the oscillations should continue, but the pressure
falls rapidly as the boundary is crossed provided the ratio of D/λ is
large. As the ratio of D/λ is reduced, the oscillations become less
pronounced and the change in pressure across the boundary of the geo-
metrical shadow also is less pronounced.

Figure 17 shows the change in pressure with lateral distance at
5 mm. from the aperture as measured for case 1 of section IV-A. Here
D/λ is small and a slight maximum at approximately 32 cm. is seen.
Then the pressure decreases rather rapidly and approaches a limit.

Figure 18 is the same measurement as was taken in figure 16 ex-
cept the frequency is that of case 3 and the ratio of D/λ is large,
on the order of 6. Note the oscillations, the rapid decrease in
pressure as the boundary of the geometrical shadow is crossed, and the
gradual decrease in pressure with the superimposed oscillations. The
calculation of the exact position of the oscillation from the theory
is a tedious operation and will not be attempted here.

Figure 17. Pressure vs. lateral distance from center of aperture at 0.5 cm. for surface, circular aperture, f = 500 cps. (See Appendix II for pressure reference level.)
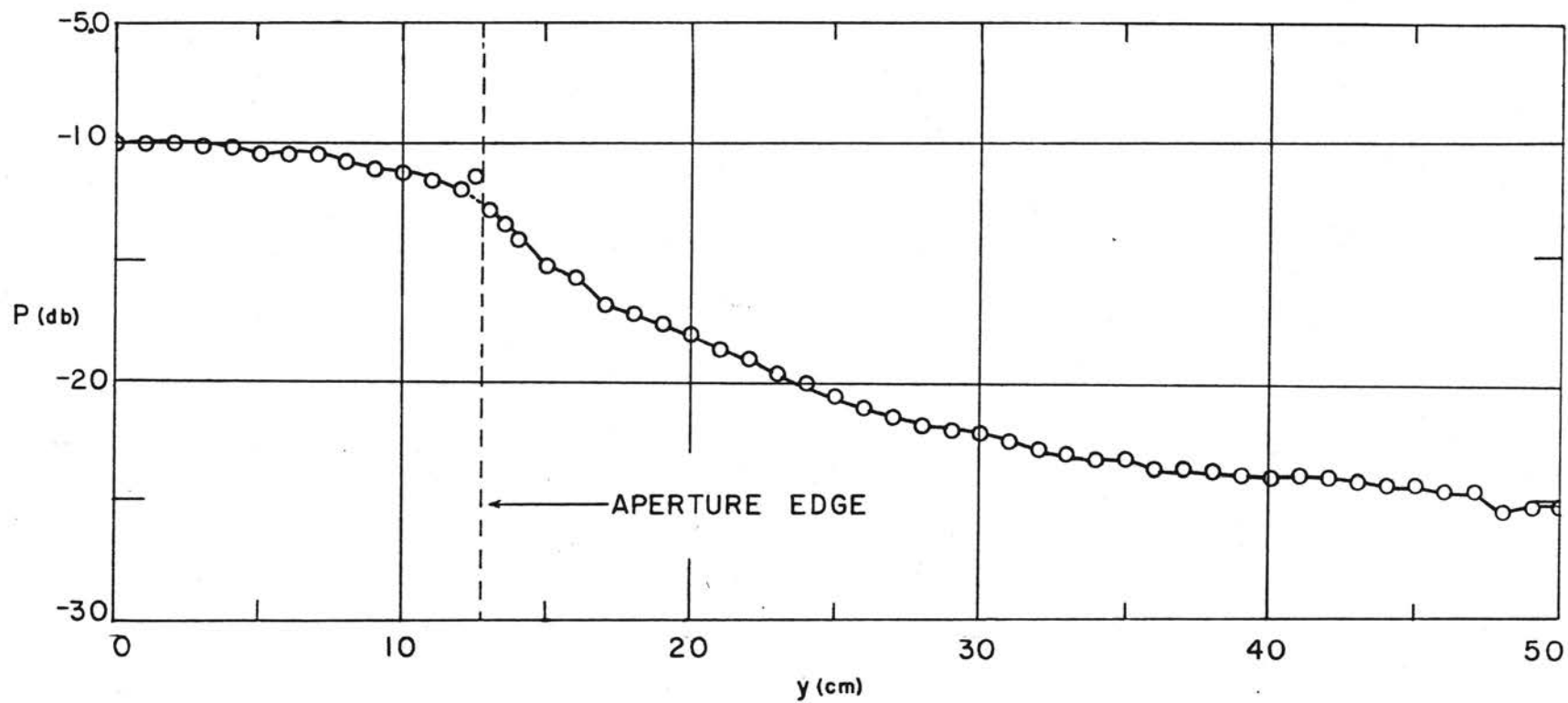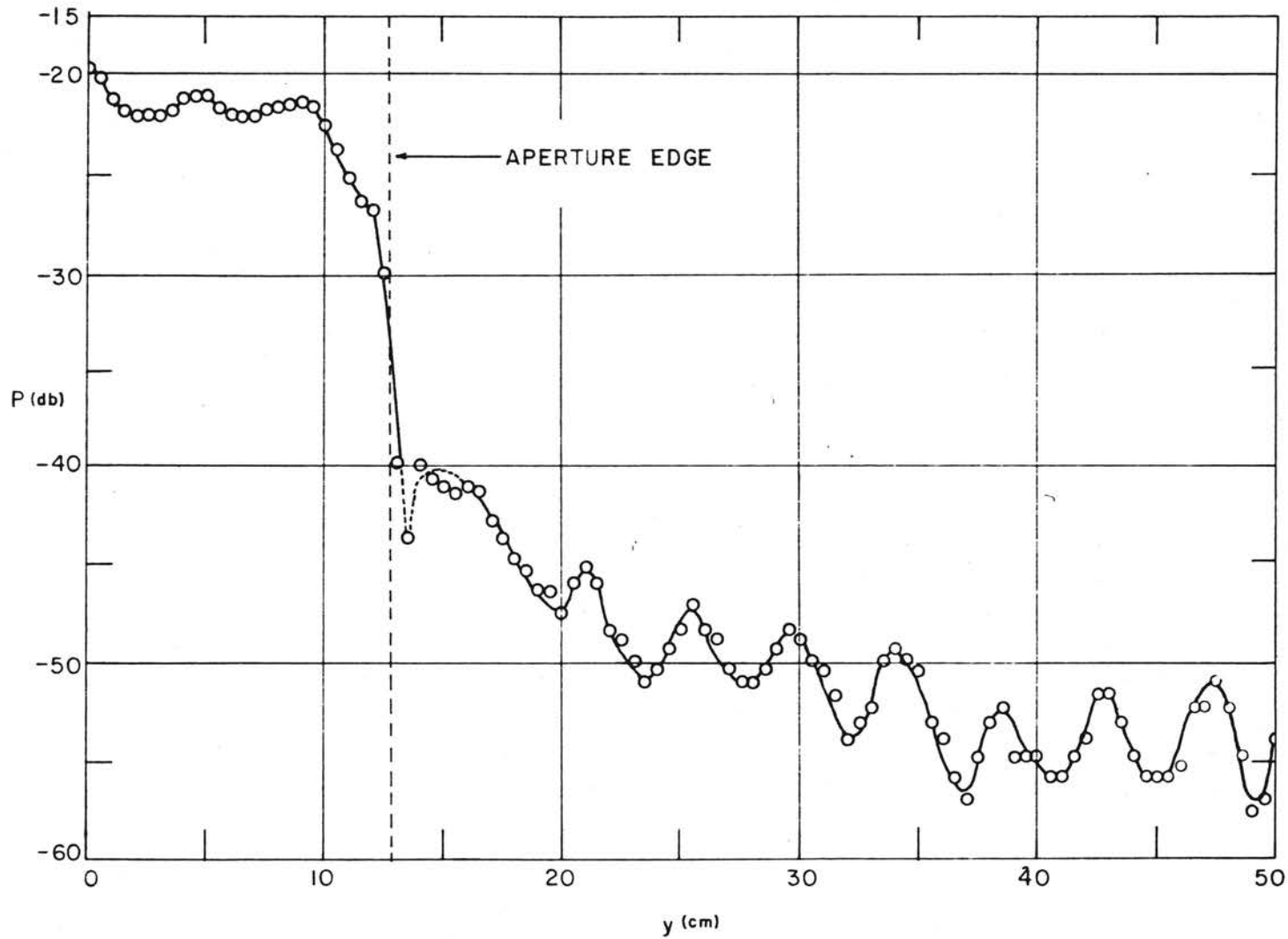
Figure 18. Pressure vs. lateral distance from center of aperture at 0.5 cm. from surface, circular aperture, f = 8000 cps. (See Appendix II for pressure reference level.)

CHAPTER V

EXTENDED STUDY OF CIRCULAR APERTURE

A. General Discussion

The pressure field measurements were extended, for case 2 of
section IV-A, to include the normal pressure gradient along the axis
and across the face of the aperture and plate. This wavelength was
chosen for the measurements because of the structure of the microphone
shown in figure 7. The ports are spaced 1.02 cm. apart; thus with
the wavelength of 26.4 cm., we are measuring an interval of 0.0391λ.
However, the wavelength can be decreased to 10 cm. before serious
difficulty should arise since the distance between ports would be 0.10
λ.

The two ports are connected to the two sides of a .0003 inch
thick aluminium membrane through approximately equal air volumes.
However, it was necessary to partially close the front port in order
to match the sensitivities of the two ports and their resonant fre-
quencies (See Appendix III).

For this case, it is necessary to assume a wave form in order
to determine the characteristics of the gradient, and pressure fields.
On the basis of the radial pressure and phase measurements shown in
figures 19 and 20 respectively, we chose a spherical wave for an
approximation to the wave form. We chose the spherical wave because
figure 19 indicates the wave to be nearly plane near the aperture but

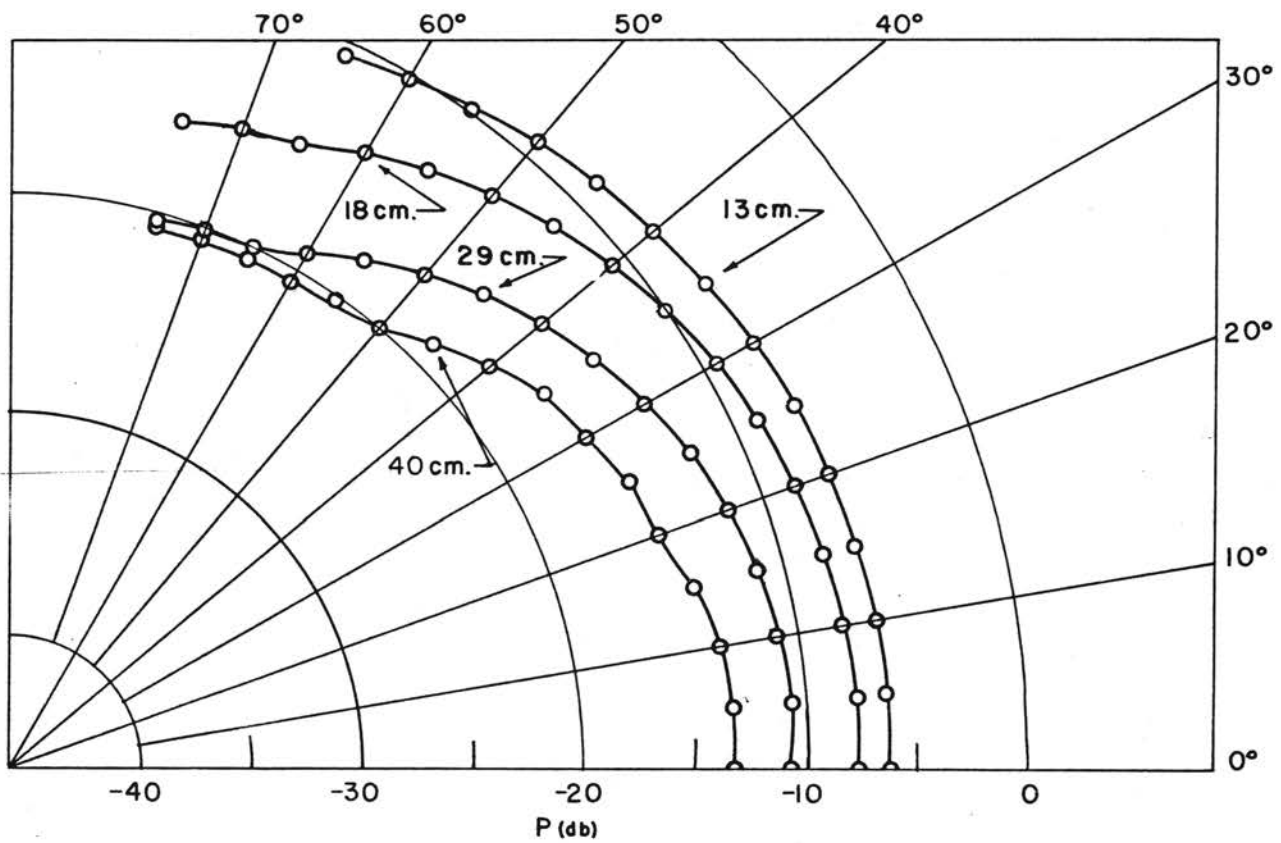Figure 19. Pressure vs. azimuthal angle, circular aperture, f = 1500 cps. (See Appendix II for pressure reference level.)
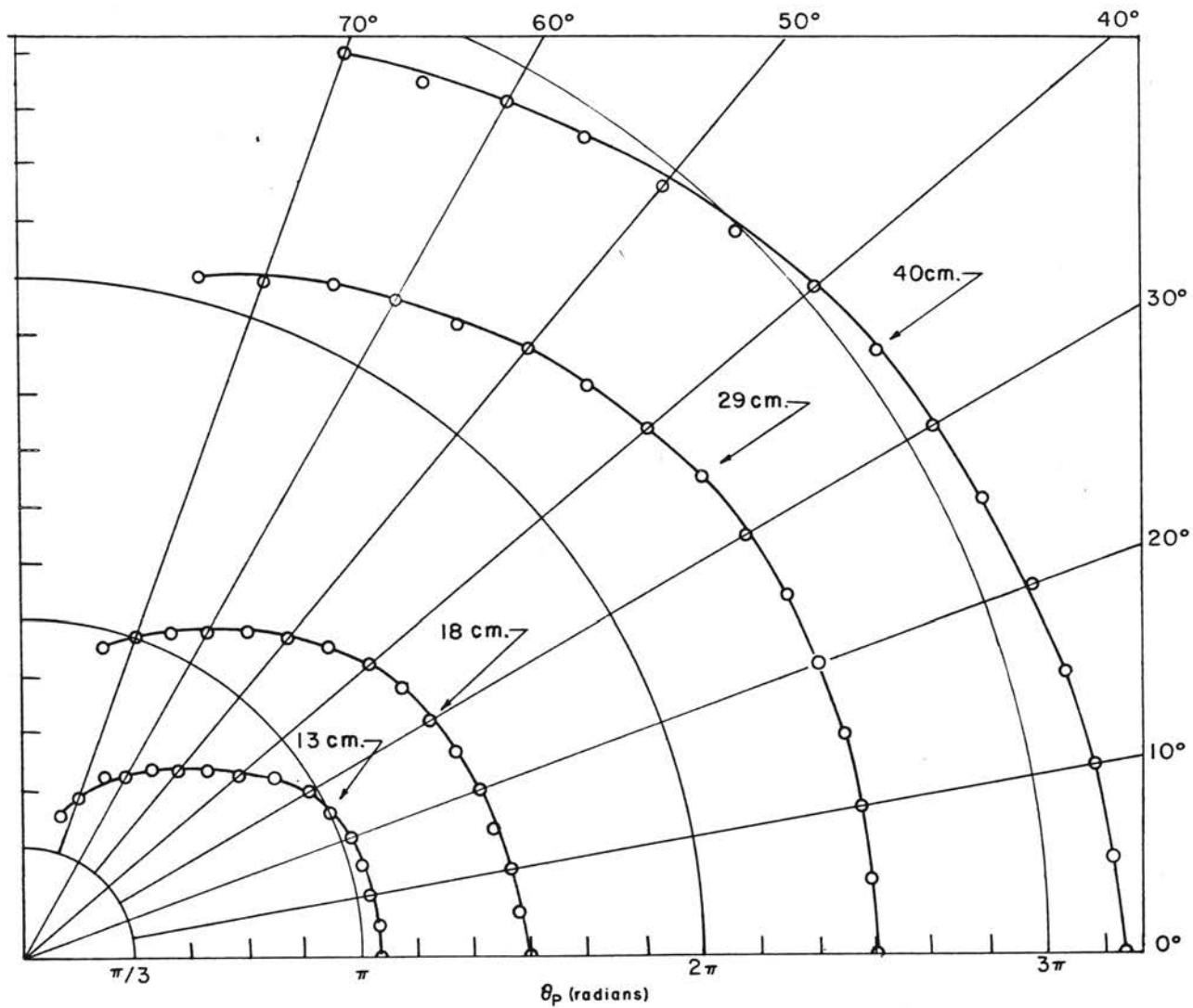
Figure 20. Phase of the pressure (relative to the phase of the oscillator output) vs. azimuthal angle, circular aperture, f = 1500 cps. (See Appendix II for pressure reference level.)

nearly spherical as it propagates out. The phase values for all phase curves are relative to the output of the oscillator. To make them relative to the pressure wave at the aperture one would shift the axis such that the phase of the pressure is zero at $\varkappa = 0$.

B. The Axial Pressure Field

Assuming a spherical wave with no attenuation the pressure at any point in the field will be given by the real part of

$$\bar{P} = \frac{P_0}{R} e^{j(\omega t - KR)} \tag{6}$$

where

$$K = \frac{2\pi}{\lambda} \quad , \quad R = (\varkappa^2 + y^2 + z^2)^{1/2} \tag{7}$$

and P_0 is the pressure at the surface, ω the angular frequency, R the distance from the aperture and K the propagation constant. Taking the real part of equation 6, and evaluation at $R = (\varkappa, 0, 0)$ we have

$$Re[\bar{P}] = \frac{P_0}{\varkappa} \cos(\omega t - K\varkappa) \tag{8}$$

From equation (8) we see that for a spherical wave the magnitude of the pressure decreases as $1/\varkappa$. Figure 21 shows the pressure as measured along the axis and the theoretical pressure for a plane and spherical wave. The oscillations appearing at 100 cm. are due to reflections primarily from the floor. Note that the wave remains fairly plane for approximately 10 cm. and then changes to a more spherical form.

Figure 22 shows the phase change of the pressure wave along the axis. From the curve we see the wave propagates uniformly. The phase change along the axis is the same for both the plane wave and the spherical wave.

C. The Pressure Gradient

The normal pressure gradient may be represented by

$$\nabla \bar{P} \cdot \bar{\iota} \tag{9}$$

where

$$\nabla \bar{P} = \bar{\iota} \frac{\partial \bar{P}}{\partial x} + \bar{J} \frac{\partial \bar{P}}{\partial y} + \bar{K} \frac{\partial \bar{P}}{\partial z}$$

and $\bar{\iota}$ is a unit vecter in the direction of the normal.

Then from equation (9)

$$\nabla \bar{P} \cdot \bar{\iota} = \frac{\partial \bar{P}}{\partial x} \tag{10}$$

Substituting equation (6) into (10)

$$\frac{\partial \bar{P}}{\partial x} = \left[-\frac{P_0}{R^2} - \frac{JKP_0}{R} \right] \frac{x}{R} e^{J(\omega t - KR)} \tag{11}$$

Evaluating equation (11) along the axis, $R = (x, 0, 0)$,

$$\frac{\partial \bar{P}}{\partial x} = \left[-\frac{P_0}{x^2} - \frac{JKP_0}{x} \right] e^{J(\omega t - Kx)} \tag{12}$$

Taking the real part of equation (12)

$$Re\left[\frac{\partial \bar{P}}{\partial x} \right] = -\frac{P_0}{x^2} \cos(\omega t - Kx) + \frac{P_0 K}{x} \sin(\omega t - Kx) \tag{13}$$
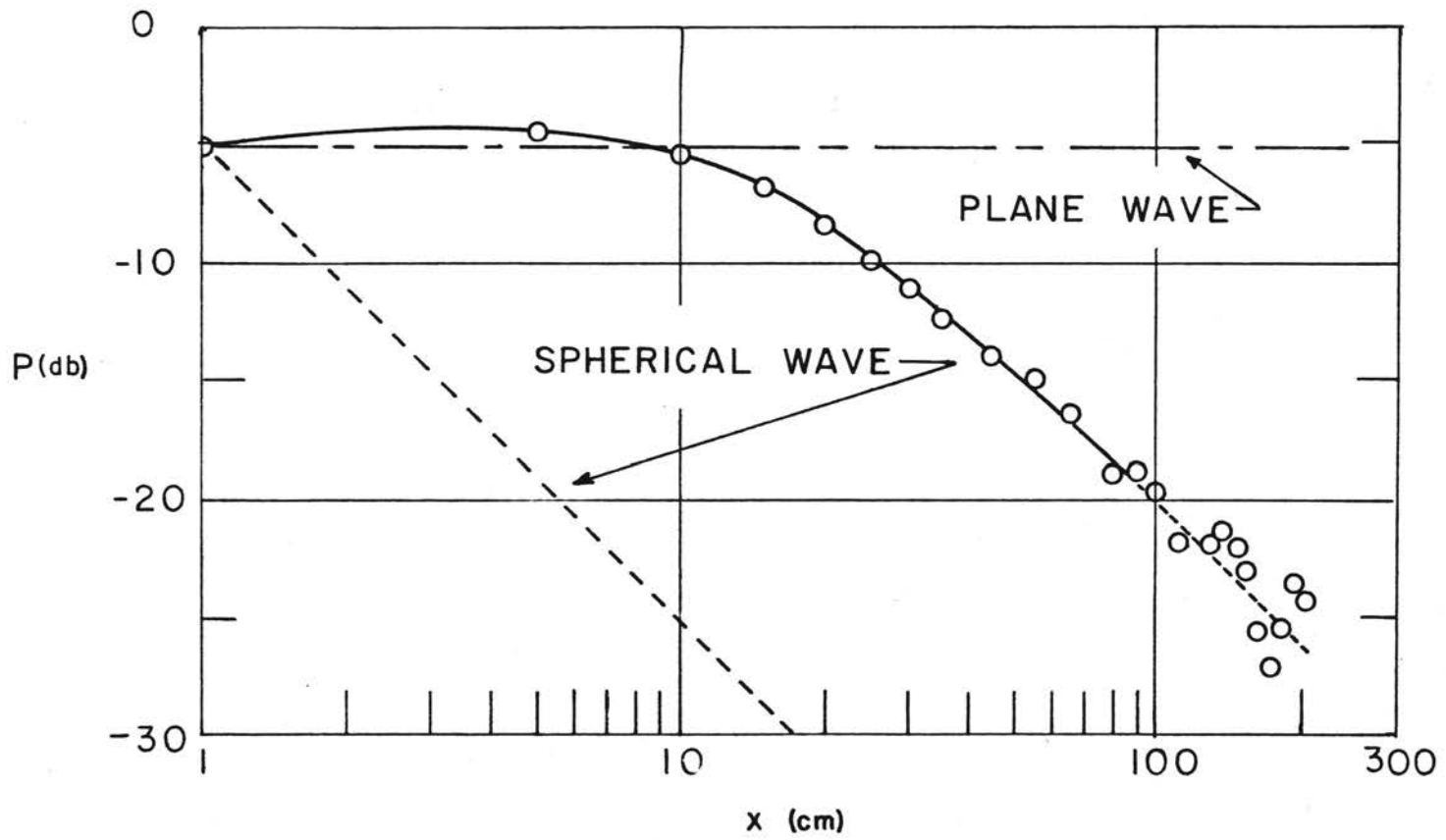
Figure 21. Pressure vs. axial distance, circular aperture, f = 1500 cps. (See Appendix II for pressure reference level.)
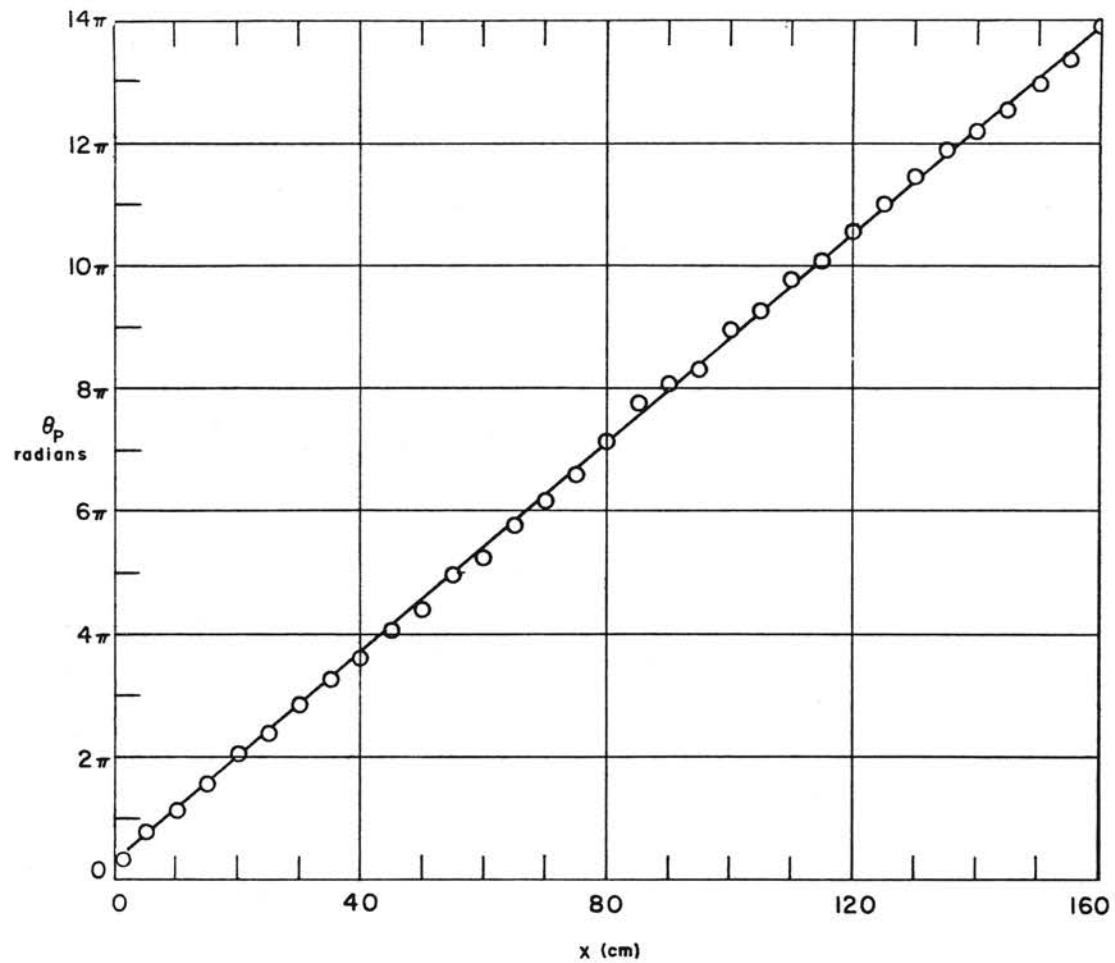
Figure 22. Phase of the pressure (relative to the phase of the
oscillator output) vs. axial distance, circular aperture,
f = 1500 cps. (See Appendix II for pressure reference level.)

Investigation of equation (13) reveals that at χ = 4.2 cm. the modulus of the two terms are equal, and at 40 cm. the modulus of the second term is large compared to the first. Thus for $\chi > 40$ cm. the gradient may be represented by

$$Re\left[\frac{\partial P}{\partial \chi}\right] = K\left(\frac{P_0}{\chi}\right) SIN(\omega t - K\chi) \qquad (14)$$

Comparing equation (14) with equation (8) we note that the amplitude of the gradient is the amplitude of the pressure attenuated by the factor K , and is 90 degress out of phase with the pressure.

Now in the region of 4.2 to 40 cm. both terms must be retained in the right member of equation (13). Considering the right member of equation (13) we can write it in the form

$$- \frac{P_0}{\chi^2} COS(\omega t - K\chi) + \frac{K P_0}{\chi} SIN(\omega t - K\chi) = C COS\left[(\omega t - K\chi) + \theta\right] \qquad (15)$$

where C is a constant and θ the phase relation to the pressure. Expanding the right member as the sum of two angles and comparing to the left member we have

$$\theta = arc\ TAN\ K\chi \qquad (16)$$

and

$$C = \frac{P_0}{\chi}\left(\frac{1}{\chi^2} + K^2\right)^{1/2} \qquad (17)$$

Figure 23 shows the gradient of the pressure as measured with the gradient microphone and the gradient of the pressure as predicted from equation (13).
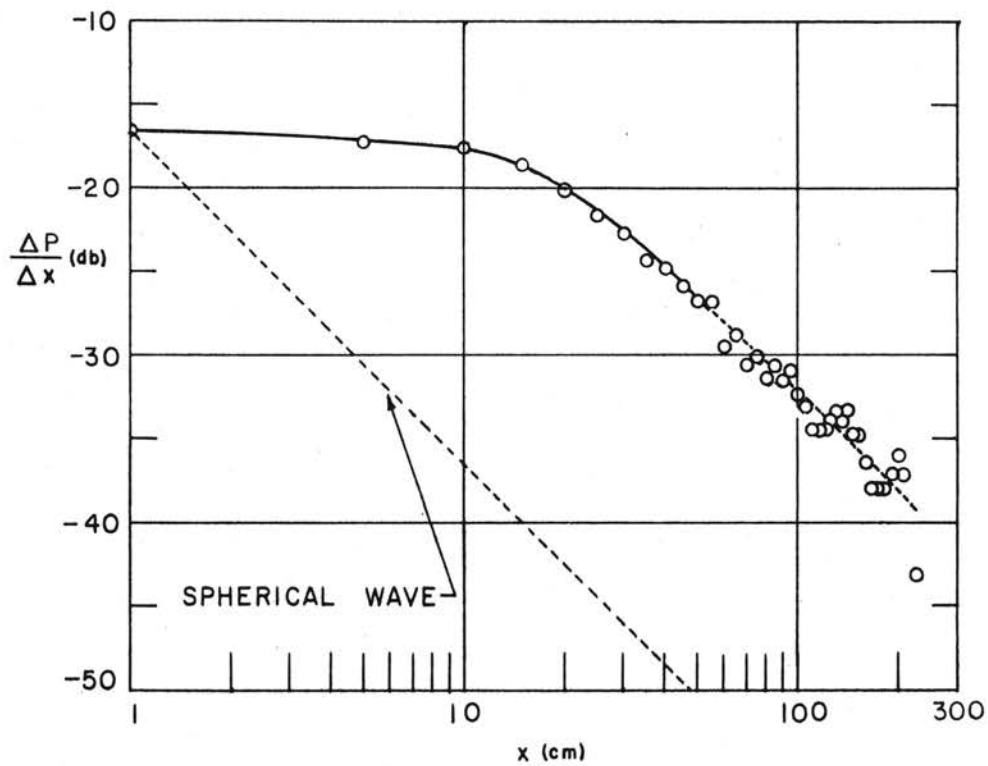
Figure 23. Gradient of the pressure vs. axial distance, circular aperture, f = 1500 cps. (See Appendix TT for pressure reference level.)
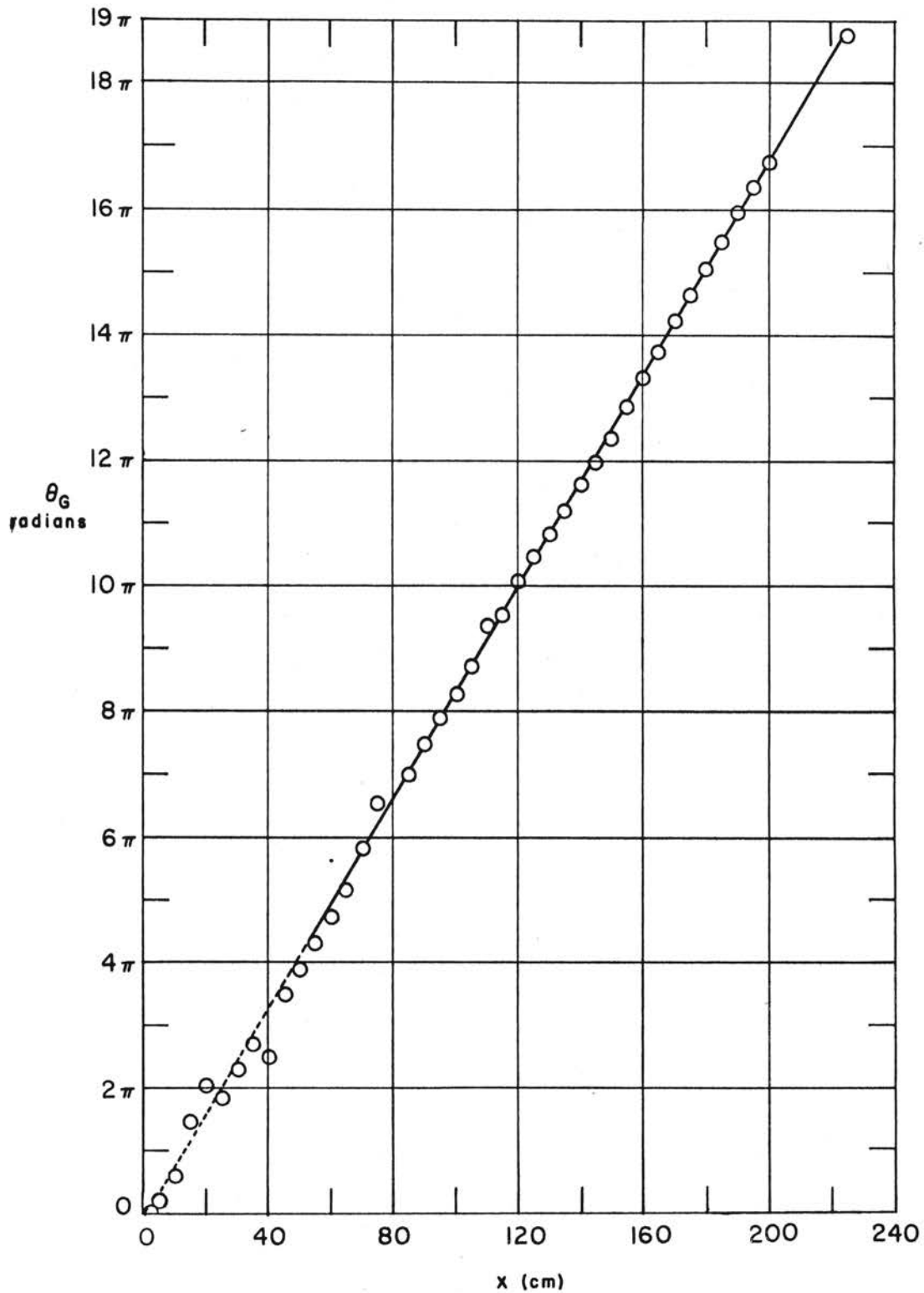
Figure 24. Phase of the pressure gradient (relative to the oscillator output) vs. axial distance, circular aperture, f = 1500 cps. (See Appendix II for pressure reference level.)

From equation (16) we see that the phase of the gradient relative to the pressure will decrease as the aperture is approached, until they are in phase at the aperture. Figure 24 shows the axial phase of the gradient as measured with the gradient microphone.

D. The Lateral Pressure Field

It is pointed out in section V-A that the pressure wave is nearly plane in the region near the aperture. This is further verified by the pressure and phase curves of the lateral field shown in figures 25 and 26. From these curves we see that the pressure and phase remain nearly constant out to 10 cm. From 10 cm. on the pressure decreases in a fashion similar to an attenuated spherical wave.

If the wave is non-attenuated and spherical the pressure will be given by the real part of equation (6) evaluated at $R = (0.5, y, 0)$ then

$$Re[\bar{P}] = \frac{P_0}{(0.25 + y^2)^{1/2}} \cos\left[\omega t - \kappa(0.25 + y^2)^{1/2}\right] \quad (18)$$

or for $y > 10\,cm$ the pressure may be approximated by

$$Re[\bar{P}] = \frac{P_0}{y} \cos(\omega t - \kappa y) \quad (19)$$

The phase of the pressure will then change linearly with y.

E. The Lateral Normal Pressure Gradient

The normal pressure gradient across the surface of the aperture and screen is given by equation (11) evaluated at $R = (0.5, y, 0)$.

Thus

$$\frac{\partial \bar{P}}{\partial \tau} = \left[-\frac{P_o}{0.25 + y^2} - \frac{jKP_o}{(0.25 + y^2)^{1/2}} \right] \frac{0.5}{(0.25 + y^2)^{1/2}} \, e^{j\left[\omega t - K(0.25 + y^2)^{1/2}\right]} \tag{20}$$

If we consider only $y > 10$, then equation (20) may be approximated by

$$\frac{\partial \bar{P}}{\partial \tau} = \left[-\frac{P_o}{y^2} - \frac{jKP_o}{y} \right] \frac{0.5}{y} \, e^{j(\omega t - Ky)} \tag{21}$$

Taking the real part of equation (21)

$$Re\left[\frac{\partial \bar{P}}{\partial \tau}\right] = -\frac{0.5 P_o}{y^3} \cos(\omega t - Ky) + \frac{0.5 K P_o}{y^2} \sin(\omega t - Ky) \tag{22}$$

For $y > 10$, the amplitude of the first term of equation (22) is small compared to the amplitude of the second term, thus the normal gradient can be further approximated by

$$Re\left[\frac{\partial \bar{P}}{\partial \tau}\right] = \frac{0.5 K P_o}{y^2} \sin(\omega t - Ky) \tag{23}$$

Comparing equation (23) to equation (19) we see that the magnitude of the pressure gradient is the same as the magnitude of the pressure attenuated by the factor $0.5K/y$ and is 90 degrees out of phase with respect to the pressure. Figures 27 and 28 show the magnitude and relative phase of the pressure gradient across the surface as measured with the gradient microphone.

Figure 25. Pressure vs. lateral distance from center of aperture at 0.5 cm. from surface, circular aperture, f = 1500 cps. (See Appendix II for pressure reference level.)
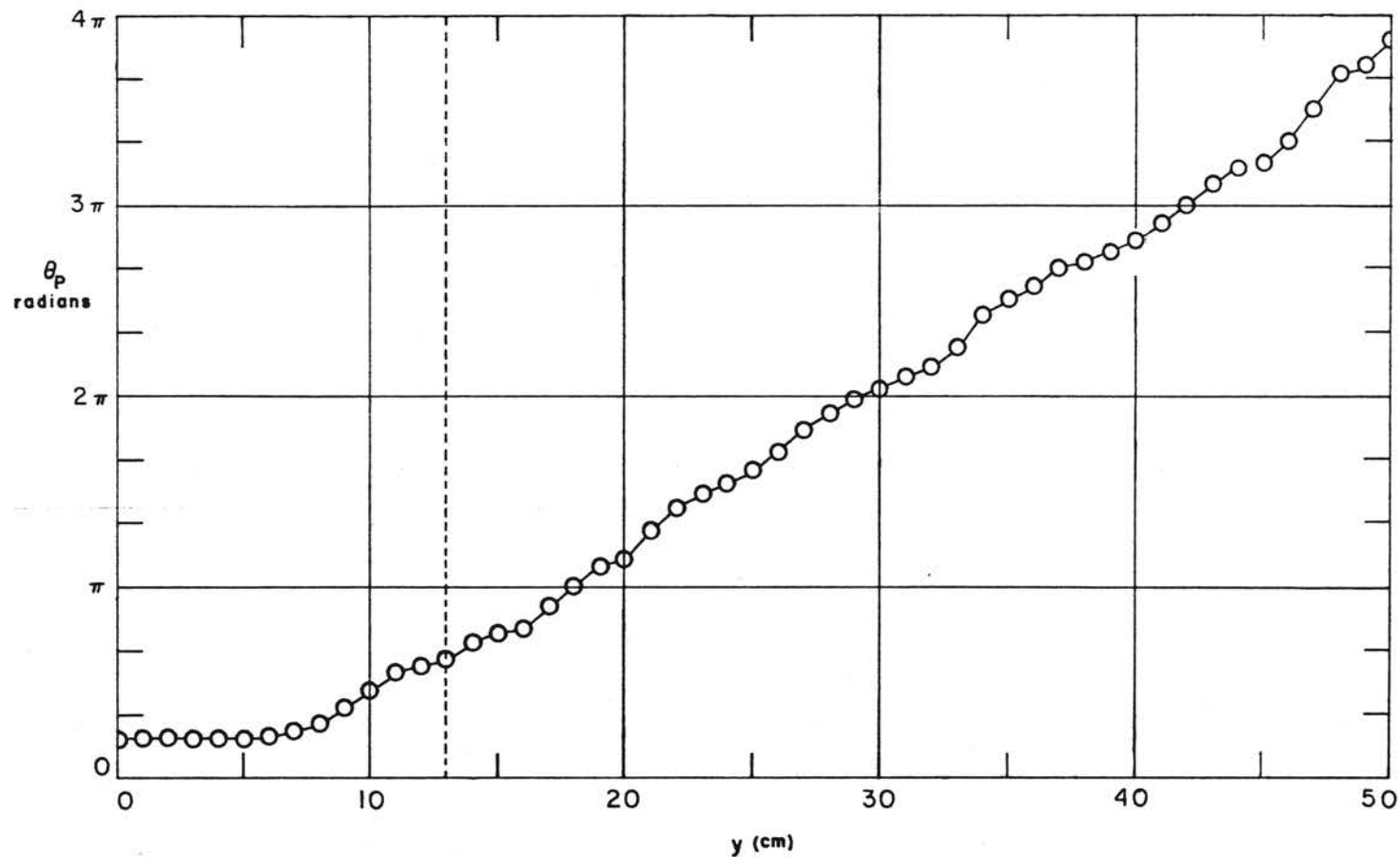
Figure 26. Phase of pressure (relative to the oscillator output) vs. lateral distance from center of aperture at 0.5 cm. from surface, circular aperture, f = 1500 cps. (See Appendix II for pressure reference level.)

Figure 27. Gradient of the pressure vs. lateral distance from center of aperture with front port 0.5 cm. from surface, circular aperture, f = 1500 cps. (See Appendix II for pressure reference level.)
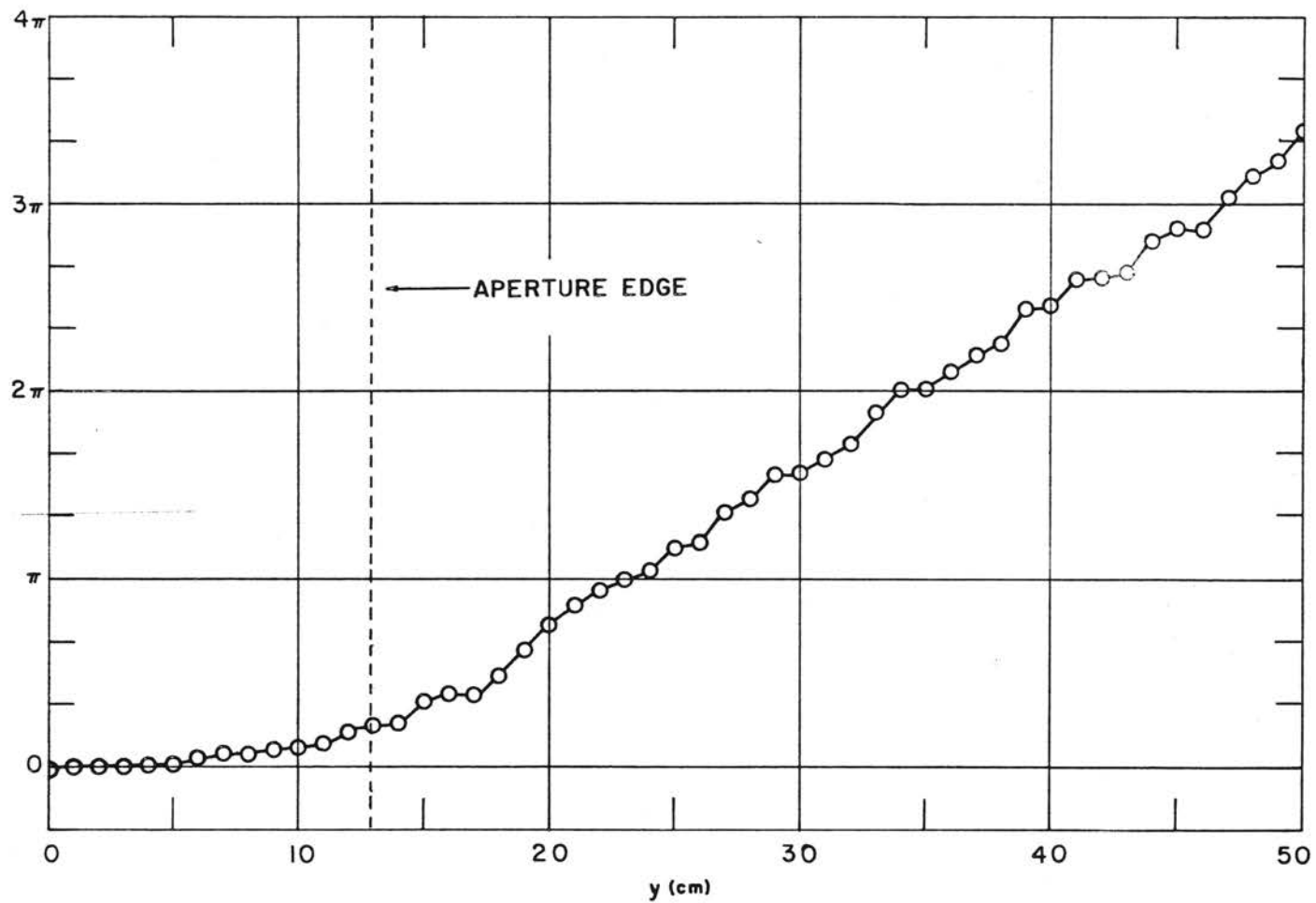
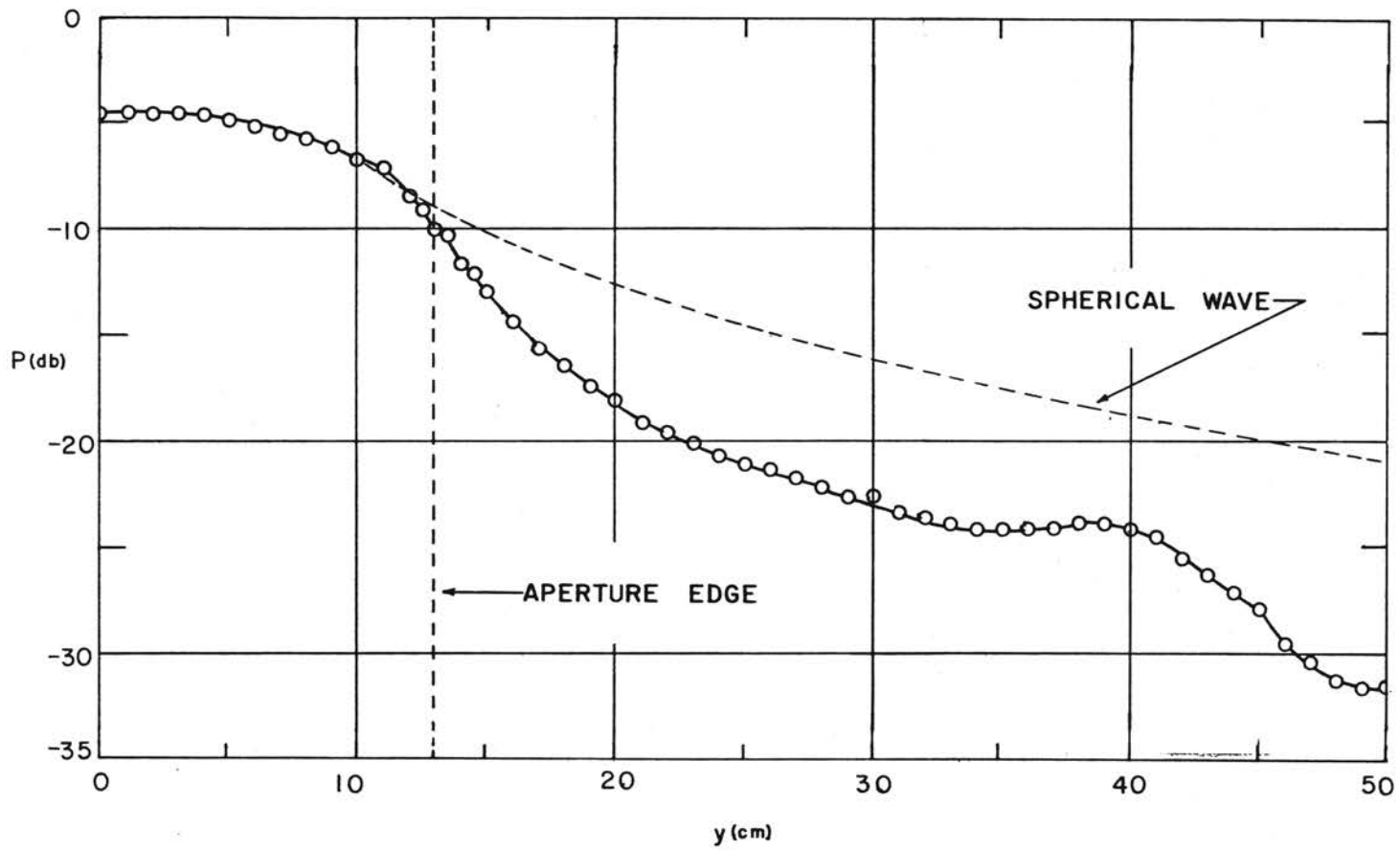Figure 28. Phase of the pressure gradient vs. lateral distance from center of aperture, with front port 0.5 cm. from surface, circular aperture, f = 1500 cps. (See Appendix II for pressure reference level.)
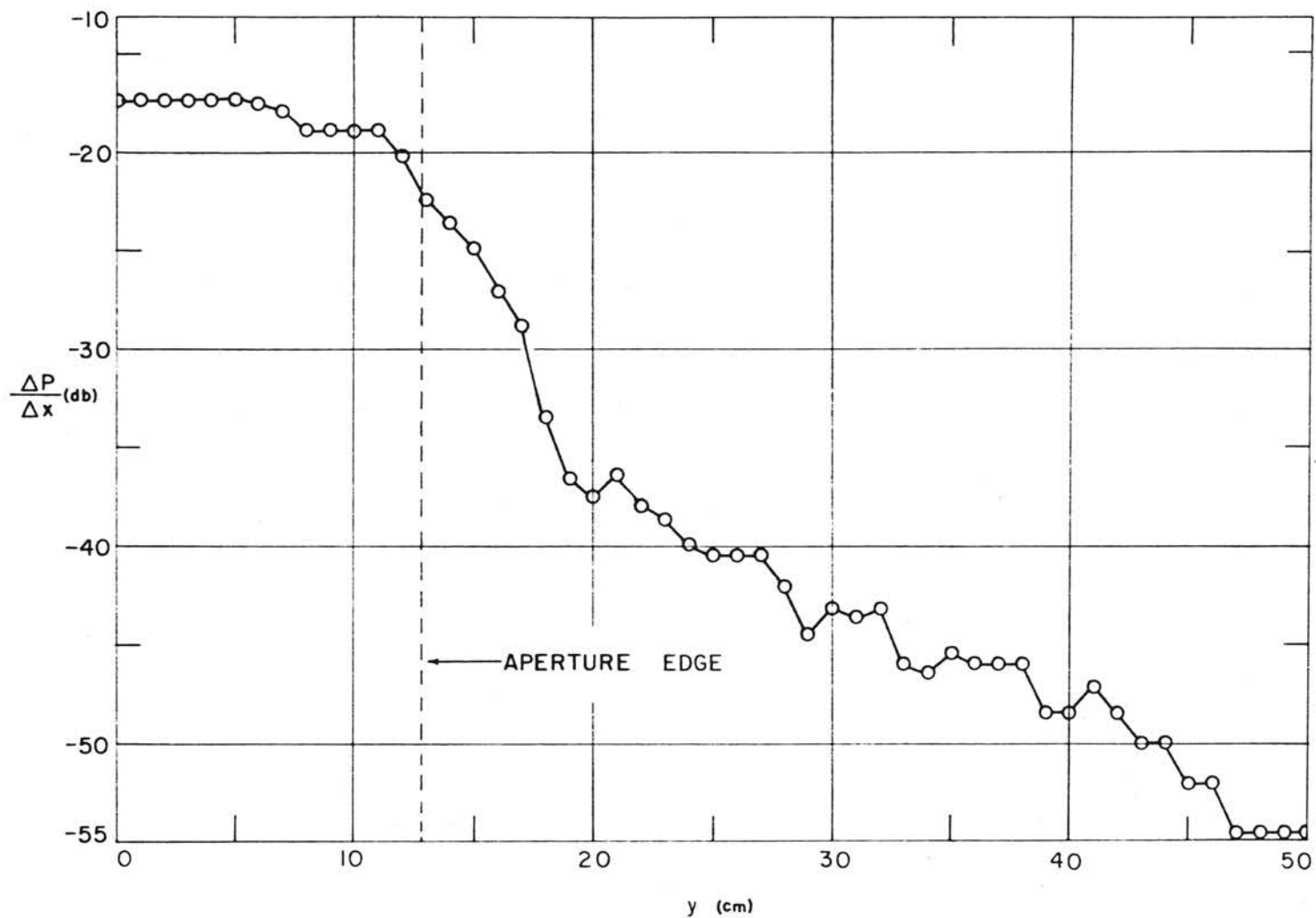
CHAPTER VI

RECTANGULAR APERTURE AND CIRCULAR DISK

A. The Radial Pressure Field of the Rectangular Aperture

The mathematical treatment[11] involving double integration over both dimensions of the wave front incident upon the aperture shows that for a length large compared to the width the result corresponds to the single slit. However, for a length comparable to the width the treatment shows that the pressure is a minimum along straight lines defined by the equations

$$\alpha = \pm n\pi \quad ; \quad \gamma = \pm n\pi \tag{24}$$

where n is an integer and α and γ are integration factors defined by

$$\alpha = \frac{\pi \ell \sin \Omega}{\lambda} \tag{25}$$

$$\gamma = \frac{\pi b \sin \phi}{\lambda} \tag{26}$$

where ℓ is the length of the aperture; b, the width of the aperture; λ, the wave length; and Ω and ϕ are angles measured from the normal to the aperture at its center in planes through the normal parallel to the sides ℓ and b respectively.

53

Consider the three cases for which measurements have been made.
For case one, for which the length of the aperture was oriented verti-
cally, $\alpha = 0$. Thus one can determine the value of ϕ for which the
pressure is minimum. From equation (26) a minimum should appear at
ϕ = 38.2° for a wave length λ = 4.95 cm., which was the wave length
used for the measurements. Figure (29) shows the measured pressure
field at 11, 50 and 90 cm.

For case two, for which the length of the aperture was oriented
horizontally, $\gamma = 0$. Hence, the values of Ω for which the
minima should occur can be determined. From equation (25), minima
should occur for

$$\Omega = 13°, 26.75°, 41.5°, 64.2°$$

Figure 30 shows the radial pressure field of the horizontal aperture
as measured for λ = 4.95 cm.

For case three, for which the length of the aperture was oriented
at an angle of 60° to the vertical, the first minima should be at a
slightly greater angle than for the horizontal case. The difference
between the angular separation of the corresponding minima will increase
as the angle from the normal increases. This is verified by the field
as shown in figure 31.

B. The Axial Field of the Rectangular Aperture

On the basis of Fresnel's theory as outlined in section IV-B, for
partially exposed zones and comparable dimensions of the rectangular
and circular aperture, one would expect the axial fields to be very
nearly the same, when the same frequencies are used. However, the maxi-
ma and minima should be shifted slightly toward the aperture and the

Figure 29. Pressure vs. azimuthal angle, rectangular aperture with major axis vertical, f = 8000 cps. (See Appendix II for pressure reference level.)

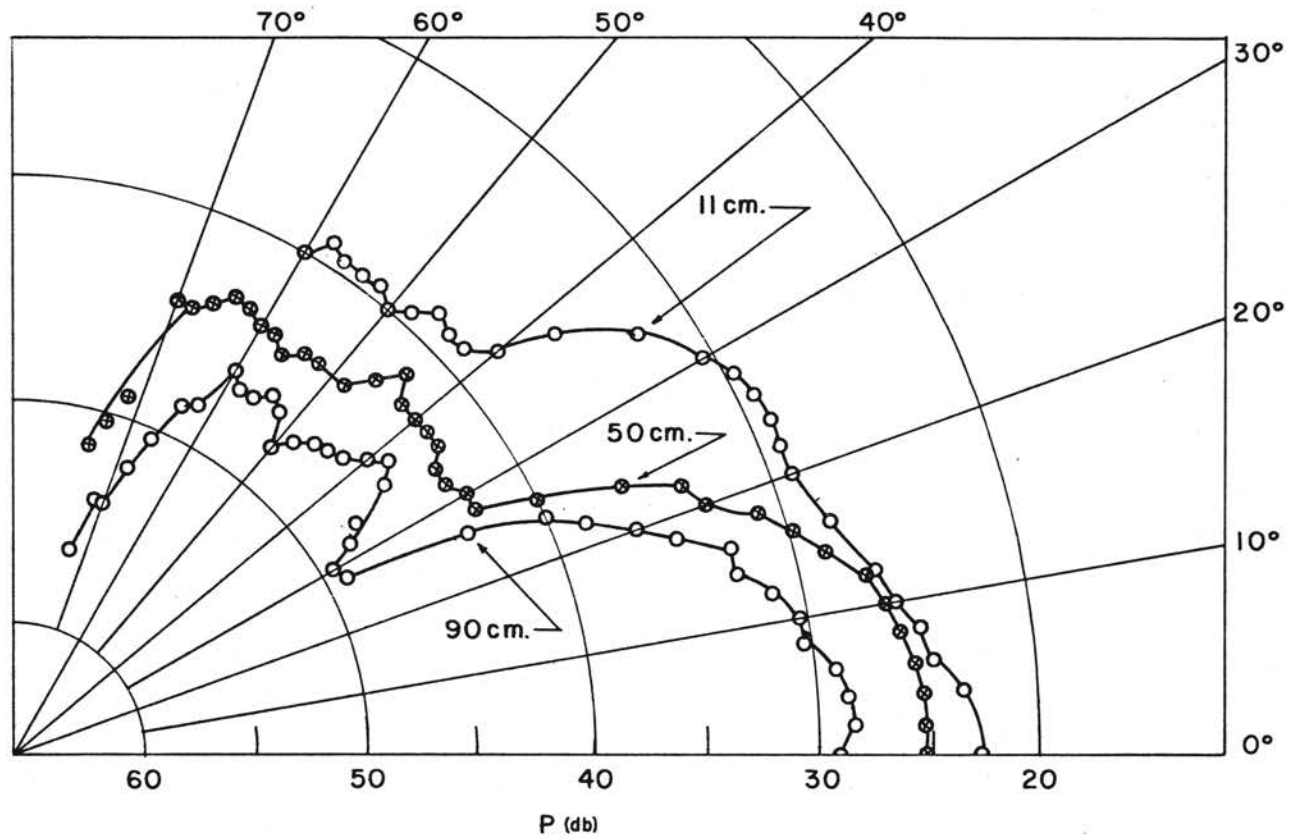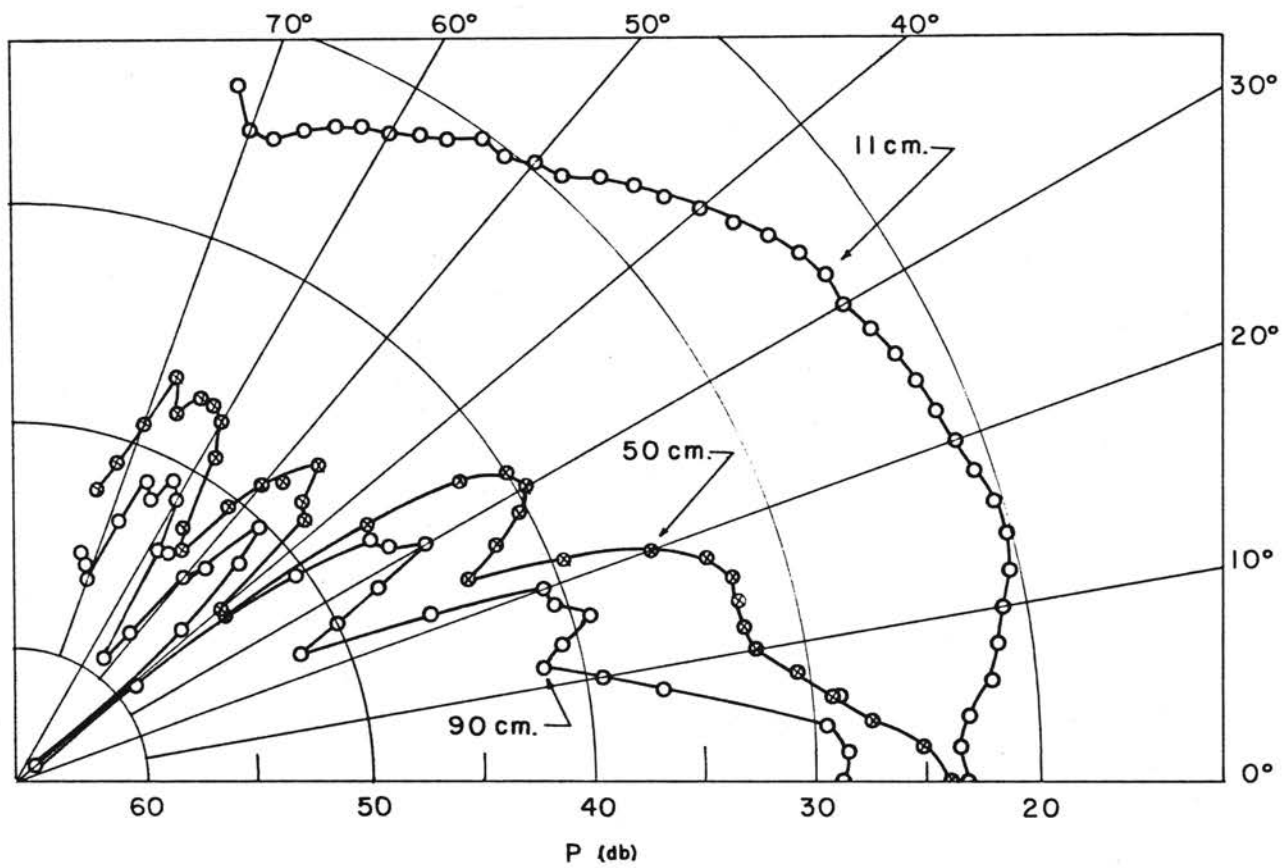Figure 30. Pressure vs. azimuthal angle, rectangular aperture with major axis horizontal, f = 8000 cps. (See Appendix II for pressure reference level.)
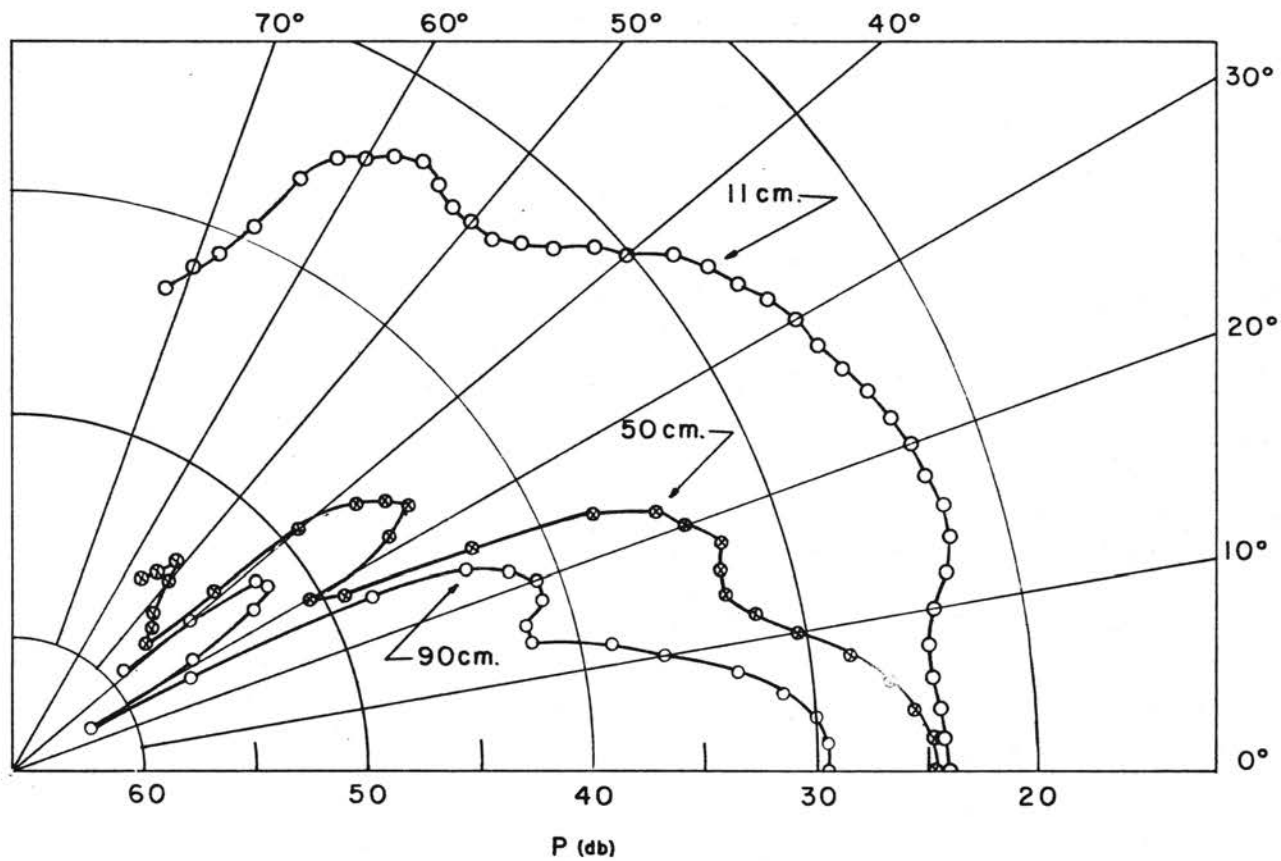
Figure 31. Pressure vs. azimuthal angle, rectangular aperture with major axis inclined at 60° to the vertical, f = 8000 cps. (See Appendix II for pressure reference level.)

average pressure to be less since the rectangular aperture is smaller. Comparisons of figure 32, with figure 16, shows this to be the case for a frequency of 8000 cps.

C. The Near Field or Lateral Pressure

Again, because of the comparable dimensions of the rectangular and circular apertures, the approximate theory as outlined in section IV-B should apply for the same frequencies. Inspection of figures 33, 34 and 35 shows this to be essentially the case for $\nu = 0.2$ cm. In figure 35 one observes that the pressure drops very rapidly as the boundary of the geometrical shadow is crossed. Note that at approximately 11 cm. in figures 33, 34 and 35 there appears an abrupt minimum. This point is $\lambda/4$ from the inside surface of the mounting rings and could possibly be due to a standing wave set up by reflections from this surface. Also over the external surface of the rings some irregularities occur which are possibly due to the interaction of the rings with the field. Otherwise, the field follows the field of the circular aperture, except the oscillations are not as great.

D. The Circular Disk

On the basis of Fresnel's formulation of the wave theory, Poisson[6] predicted the existence of an axial bright spot behind a circular disk illuminated by a point source on its axis. This bright spot was first observed by Arogo, and his observation gave the wave theory much support.

The Kirchhoff[12] theory expresses the pressure at points within a region of space in terms of assumed boundary values of the surface bounding the region. The Maggi transformation reduces the Kirchhoff
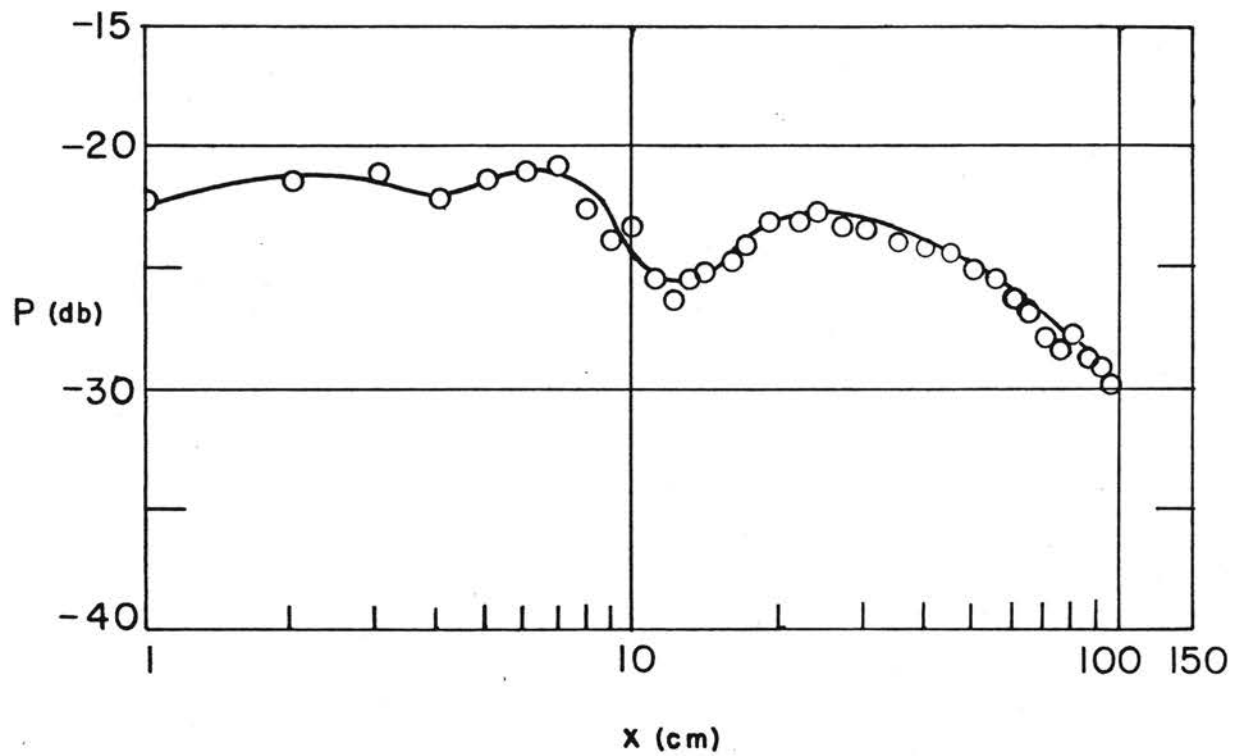
Figure 32. Pressure vs. axial distance, rectangular aperture, f = 8000 cps. (See Appendix II for pressure reference level.)

Figure 33. Pressure vs. lateral distance from center of aperture at 0.2 cm. from surface of rings, rectangular aperture with major axis vertical, f = 8000 cps. (See Appendix II for pressure reference level.)

Figure 34. Pressure vs. lateral distance from center of aperture at 0.2 cm. from surface of rings, rectangular aperture with major axis horizontal, f = 8000 cps. (See Appendix II for pressure reference level.)
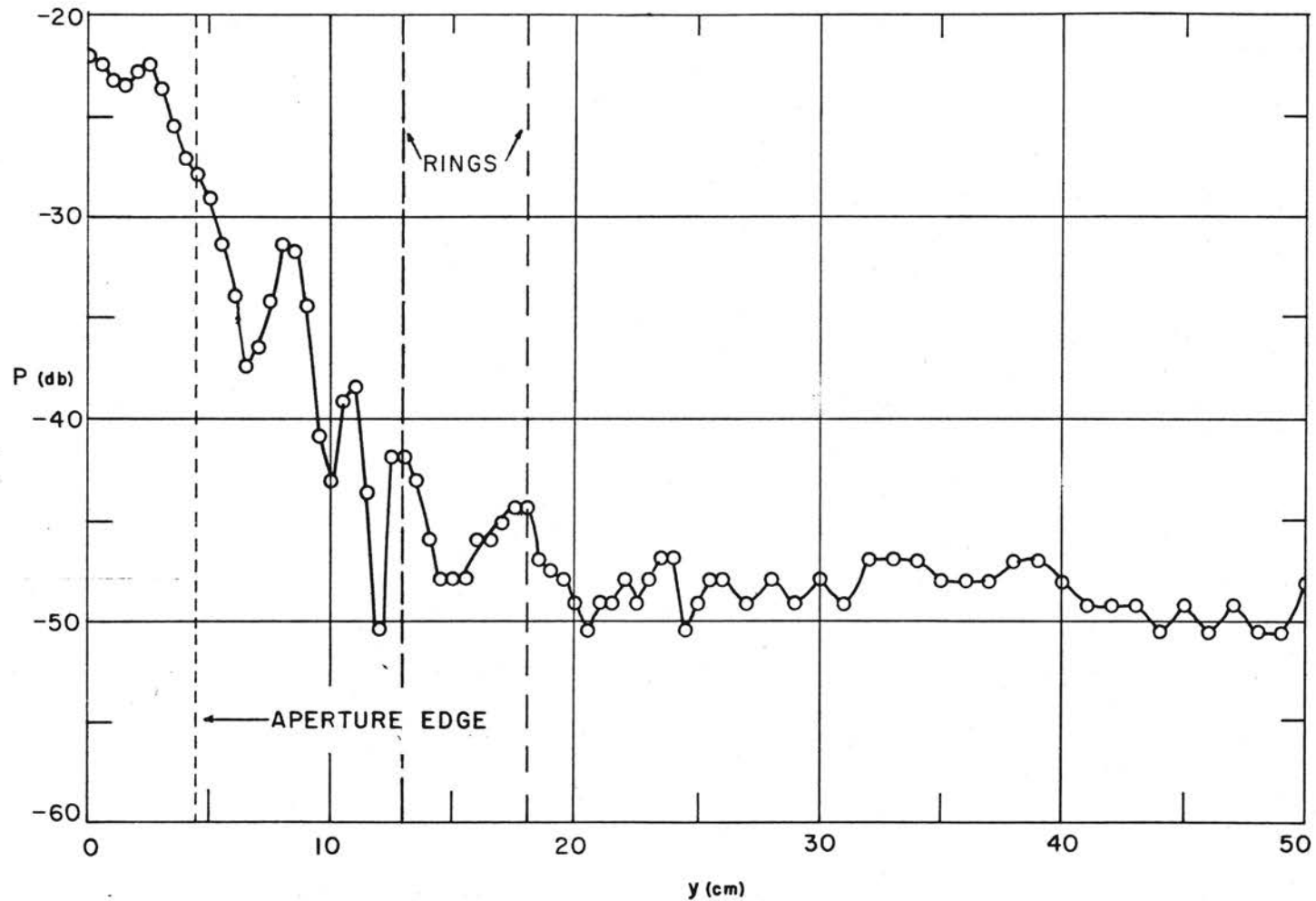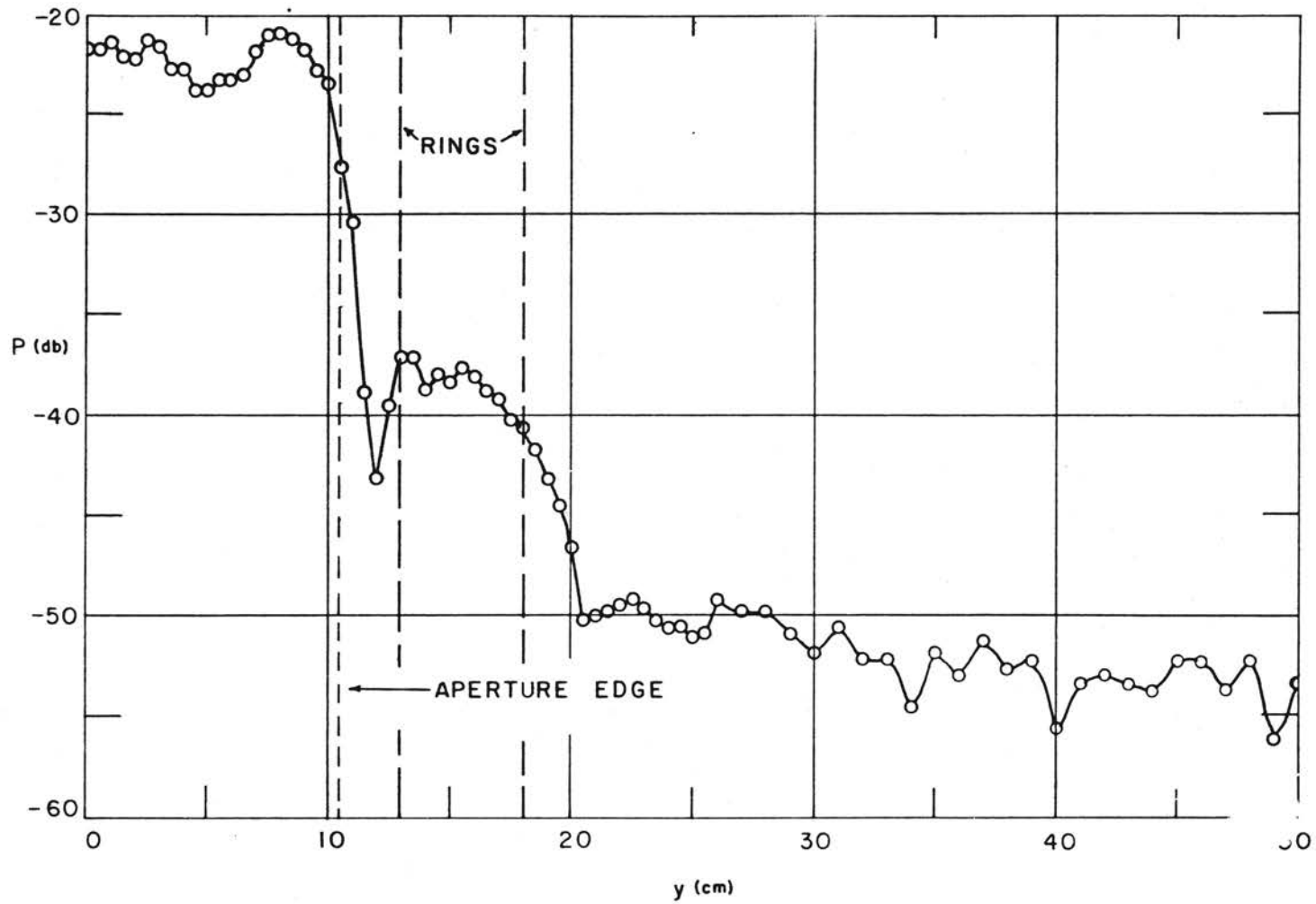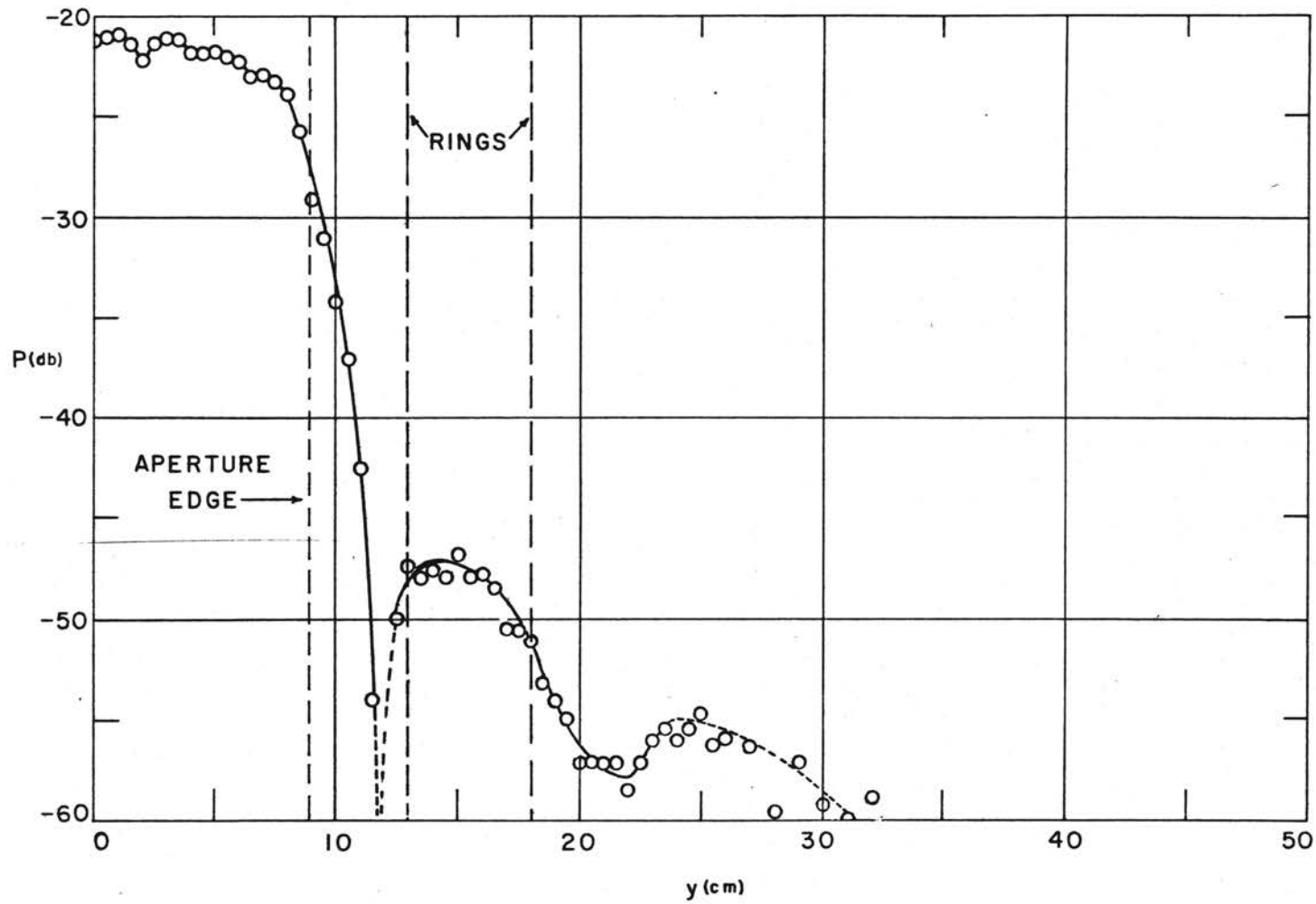
Figure 35. Pressure vs. lateral distance from center of aperture at 0.2 cm. from surface of rings, rectangular aperture with major axis inclined at 60° to the vertical, f = 8000 cps. (See Appendix II for pressure reference level.)

surface integral, in the manner of Stokes theorem, and greatly facili-
tates calculation. In addition, it exhibits with particular clarity
the difference between physical and geometrical acoustics indicating
that diffractions around an obstacle arises from waves originating at
its rim. This transformation further shows that the Kirchhoff theory
fails to distinguish between the kinds of obstacles and their shapes.

Henry Primkoff, Martin Klein, Joseph Keller and E. L. Carstensen[13]
have used the Maggi transformation to determine the pressure field on
the axis of the disk and in a plane perpendicular to the axis. They
have made measurements in water to partially verify their results.
They show that there is a central zone surrounding the axis, and sym-
metric about it, in which the pressure is high, corresponding to the
bright spot as predicated first by Poisson. This "bright spot" has a
diameter on the order of a wave length immediately behind the disk
and increases in diameter with increasing distance from it.

Around this "bright spot" there is an axially symmetric region in
which the sound pressure is on the whole low. This is called the
"physical shadow," as distinguished from the "geometrical shadow,"
which is an infinite cylinder whose base is the disk.

The sound pressure in the "physical shadow" undergoes a periodic
variation as a function of distance from the axis.

The "physical shadow" is bounded on the outside by a region of
high sound pressure. The cross section of the outer region of high
pressure between the physical and geometrical shadows, called the
"annular ring," also increases in width with increasing distance behind
the disk. At a distance on axis behind the disk of $\gamma = a^2/\lambda$,
where a is the radius of the disk and λ the sound wave length,

the bright spot and annular ring meet and the physical shadow ceases to exist.

Their results further show that at moderate distances behind the disk ($\varkappa \angle a^2/\lambda$). The pressure at the geometrical shadow boundary, ($y = a$) is approximately $\frac{1}{2}$ of the value it would have if the disk were not present. For large distances behind the disk ($\varkappa > a^2/\lambda$) the pressure at the geometrical shadow is the same as its value when the disk is not present.

The position of the outer edge of the physical shadow may be determined from the equation

$$ y = a - \frac{1}{2}\left(\frac{\lambda \varkappa}{2}\right)^{1/2} , \quad \text{for} \quad \left(\frac{a^2}{\lambda \varkappa} > 1\right) \tag{27} $$

Now using this approximate theory of Primkoff and others for the 36 cm. disk considered, the field behind the disk should become the same as the undisturbed field at a distance, $\varkappa = 65.4$ cm. at this distance the physical shadow will have disappeared. It is seen from figure 36 that the measured pressure field corresponds closely to this value; i.e., it remains high and increases with $\varkappa$, until the no field condition is reached in the region of 65 to 75 cm.

The lateral pressure measurements were taken at $\varkappa = 0.2$ cm. This distance satisfies the requirement $\varkappa \angle a^2/\lambda = 65.4$ cm. From figure 37 it is seen that the pressure is on the order of $\frac{1}{2}$ its value without the disk.

The outer edge of the physical shadow is determined from equation (27) and is located at $y = 17.25$ cm.

It is seen from figure 37 that at $y = 17.25$ cm. the pressure has increased greatly. Two probable reasons the calculated value does not

correspond to the measured value are that the condition ($\left[a^2/\lambda\tau\right]^{1/2} > 1$)
is not sufficiently satisfied, and the condition of the rigid disk are
not met. The extreme oscillations of the field behind the disk are
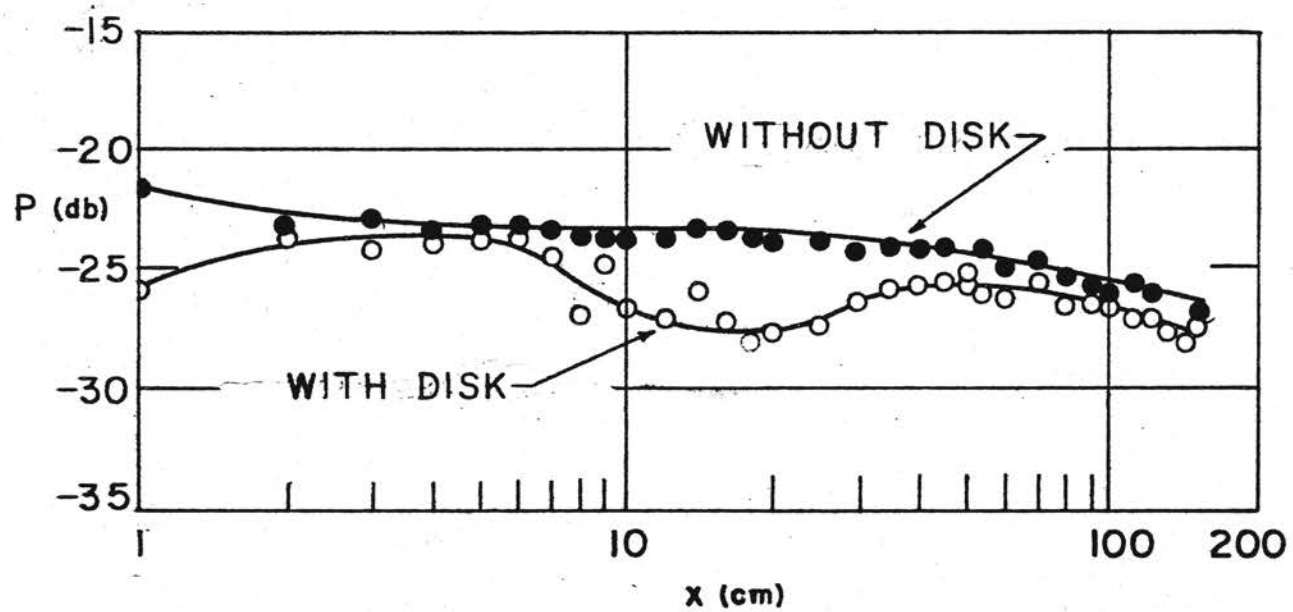possibly due to surface motions of the disk.

Figure 36. Pressure vs. axial distance, circular disk 1.5 cm. from source, f = 8000 cps. (See Appendix II for pressure reference level.)
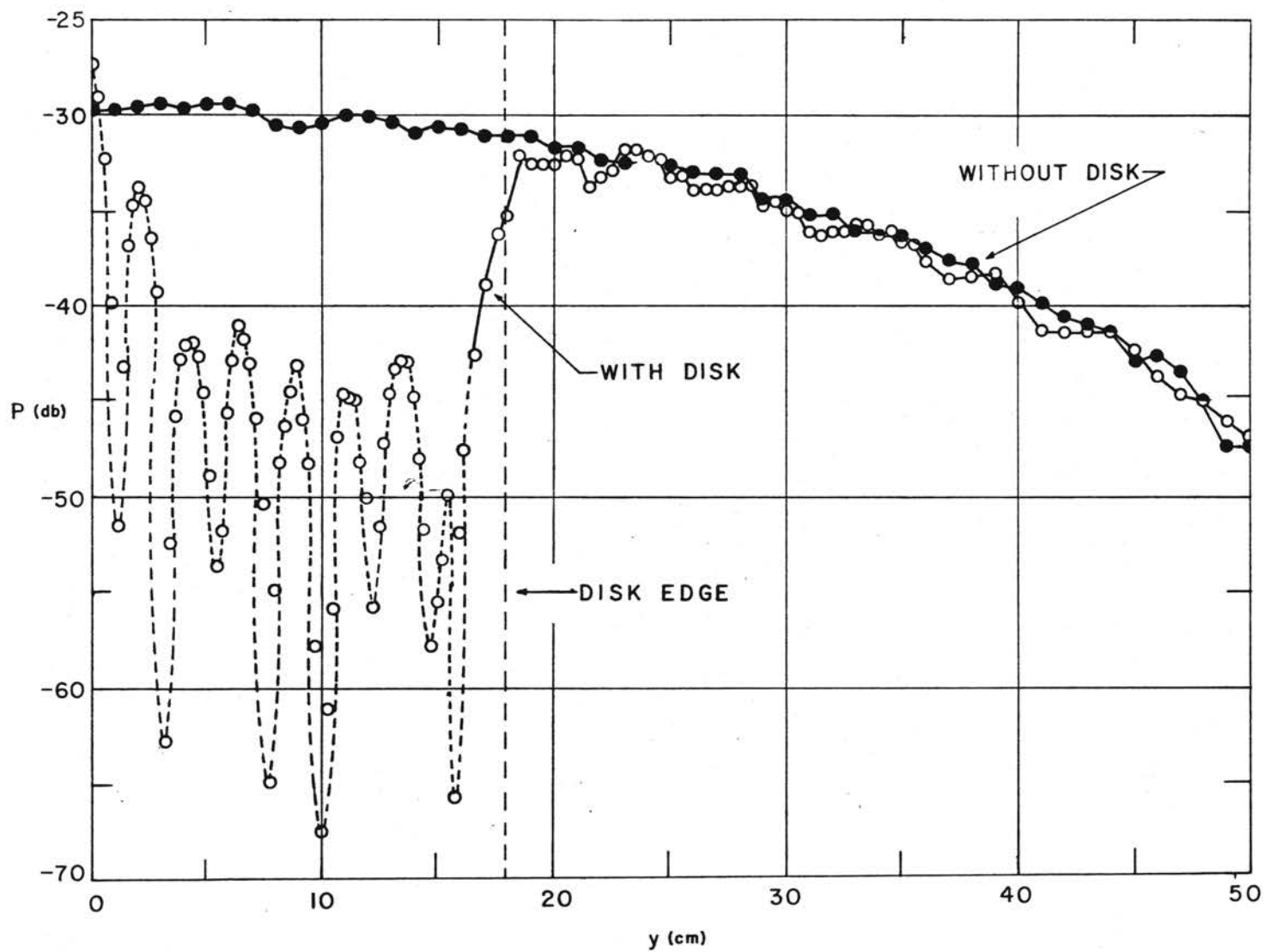
Figure 37. Pressure vs. lateral distance from center of disk at 0.2 cm. from surface, circular disk 1.5 cm. from source, f = 8000 cps. (See Appendix II for pressure reference level.)

CONCLUSION

The experimental results show good agreement with those predicted
by elementary theories, where it is expected that these theories should
apply. The pressure fields of the circular and rectangular apertures
follow the predicted field closely for far field points, that is at
distances large compared to the dimensions of the apertures. However,
near the aperture these theories are not adequate and one must use the
exact theories of Spence[3] and others for the near field determinations.
The pressure field of the circular aperture with dimensions comparable
to the wavelength agrees qualitatively with the field predicted by
theory, as does the pressure field of the circular disk.

SUGGESTIONS FOR FURTHER STUDY

The field measurements of the scattering by the disk should be
extended to include measurements on both the source and field sides of
the disk. The phase measurements across the surfaces of the disk will
reveal more information concerning the motions of the surface. Also,
similar measurements should be made with various types of disks such
as metal, plastic, rubber, etc.

The techniques of measurement used for this experimental investi-
gation may also be used to obtain data for far field predictions from
near field measurements as described by Dr. G. B. Thurston[14] in his
report, "A Method of Determination of the Radiated Acoustic Field of a
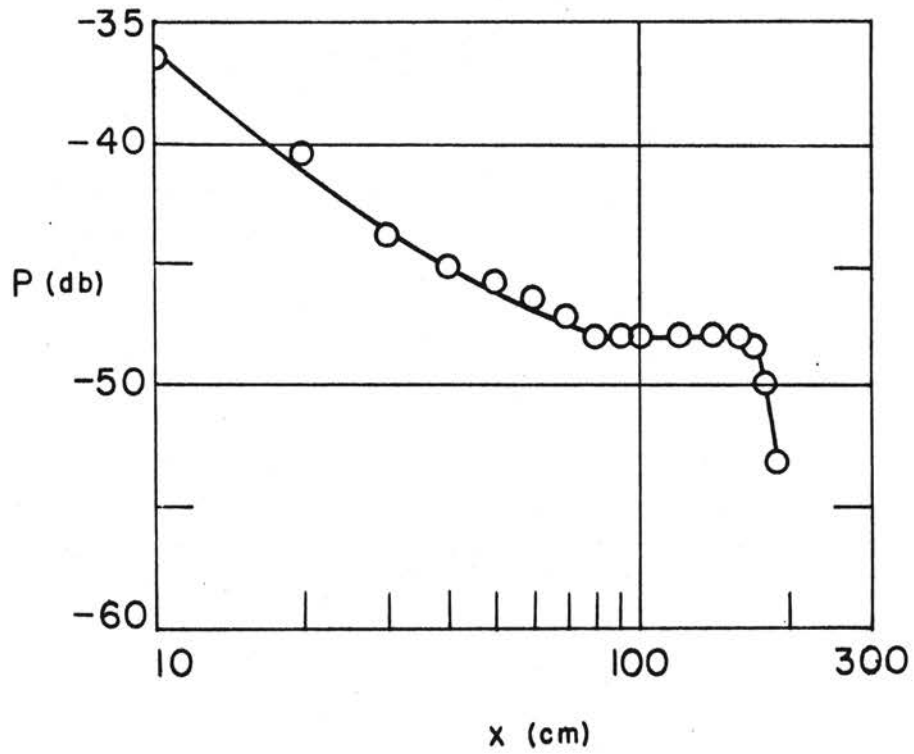Source Transmitting Through a Finite Plate."

LIST OF REFERENCES

1. Rayleigh, Lord, The Theory of Sound, Macmillan Co., New York, Vol. 2, 139 (1878).

2. Bouwkamp, C. J., "Theoretische En Numerieke Behandeling Van Buiging Door Een Ronde Opening," Dissertation, University of Groningen (1941).

3. Spence, R. D., "The Diffraction of Sound by a Circular Disk," J. Acoust. Soc. Am., 20, 380 (1948).

4. Wergeland and Stoeruste, "On Two Complementary Diffraction Problems," Phys. Rev., 73, 1397 (1948).

5. Kiver, M. S., Transistors in Radio and Television, McGraw Hill, New York, 3rd Ed., 227 (1959).

6. Rossi, B., Optics, Addison Wesley, Cambridge, 161 (1957).

7. Sears, F. W., Optics, Addison Wesley, Cambridge, 221 (1949).

8. Jenkins, F. A. and White, H. E., Fundamentals of Optics, McGraw Hill, New York, 3rd Ed., 288 (1957).

9. Spence, R. D., "Notes on the Kirchhoff Approximation in Diffraction Theory," J. Acoust. Soc. Am., 21, 98 (1949).

10. Bekefi, G., "Diffraction of Sound by a Circular Aperture," J. Acoust. Soc. Am., 25, 205 (1953).

11. Wood, R. W., Physical Optics, Macmillan Co., New York, 2nd Ed., 195 (1921).

12. Baker, B. B. and E. T. Copson, The Mathematical Theory of Huggen's Principle, Oxford University Press, New York, 2nd Ed. (1953).

13. Primakoff, H., et. al., "Diffraction of Sound Around a Circular Disk," J. Acoust. Soc. Am., 19, 132 (1947).

14. Thurston, G. B., "A Method of Determination of the Radiated Acoustic Field of a Source Transmitting Through a Finite Plate," University of Michigan, Willow Run Laboratories (1959).

APPENDICES

APPENDIX I

It is practically impossible to construct a simple acoustically opague baffle. Thus, measurements of the leakage through the chamber were made in the following manner. A plug was made of the same material as the box and inserted into the aperture. The lateral and axial measurements were then repeated for frequencies of 500 and 1500 cps. Figures 38 and 39 show the measured leakage for 500 cps, and figures 40 and 41 show the measured leakage for 1500 cps. A comparison of figures 38 through 41 with their respective pressure field curves presented in figures 15, 17, 22 and 25 shows the level of the leakage signals to be from 30 db to 40 db below the level of the measured pressure fields, so that the character of the field curves is not effected by the leakage signal.

Figure 38. Leakage pressure vs. axial distance from center of aperture at 0.5 cm. from surface, circular aperture, f = 500 cps.
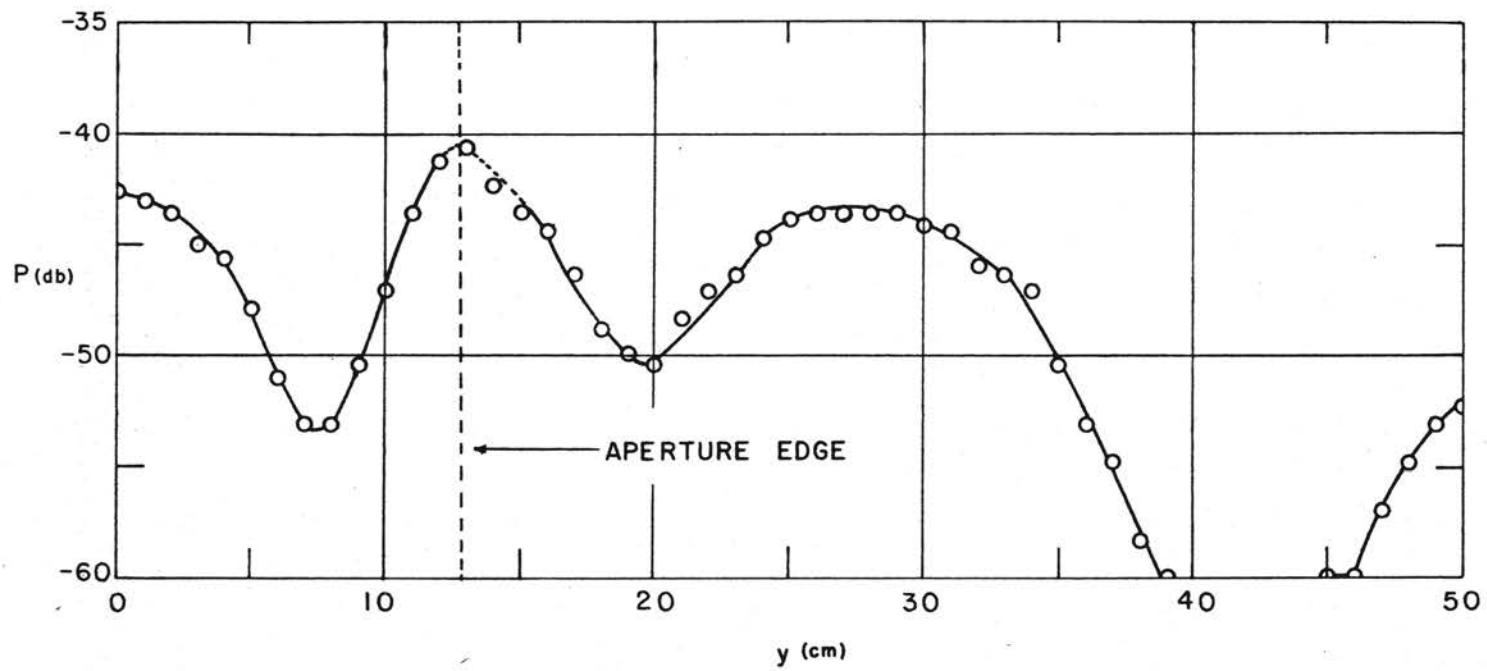
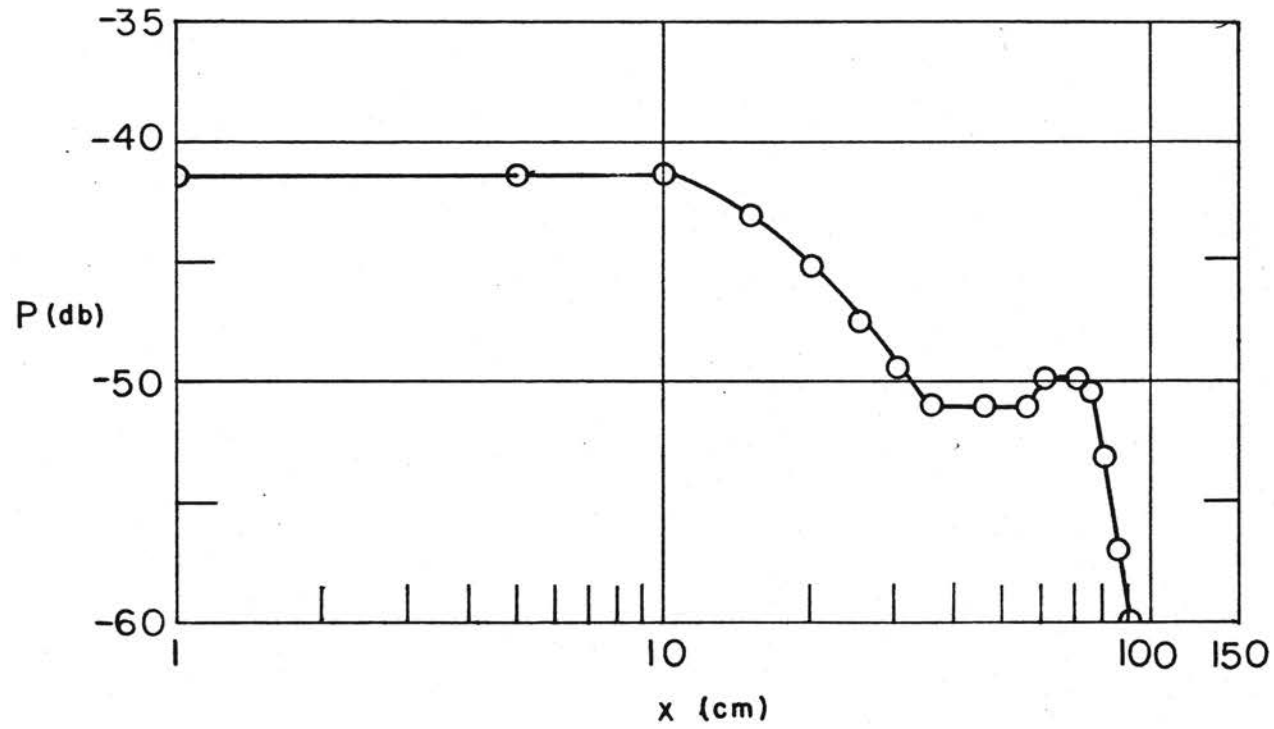Figure 39. Leakage pressure vs. lateral distance, circular aperture, f = 500 cps.

Figure 40. Leakage pressure vs. axial distance from center of aperture at 0.5 cm. from surface, circular aperture, f = 1500 cps.
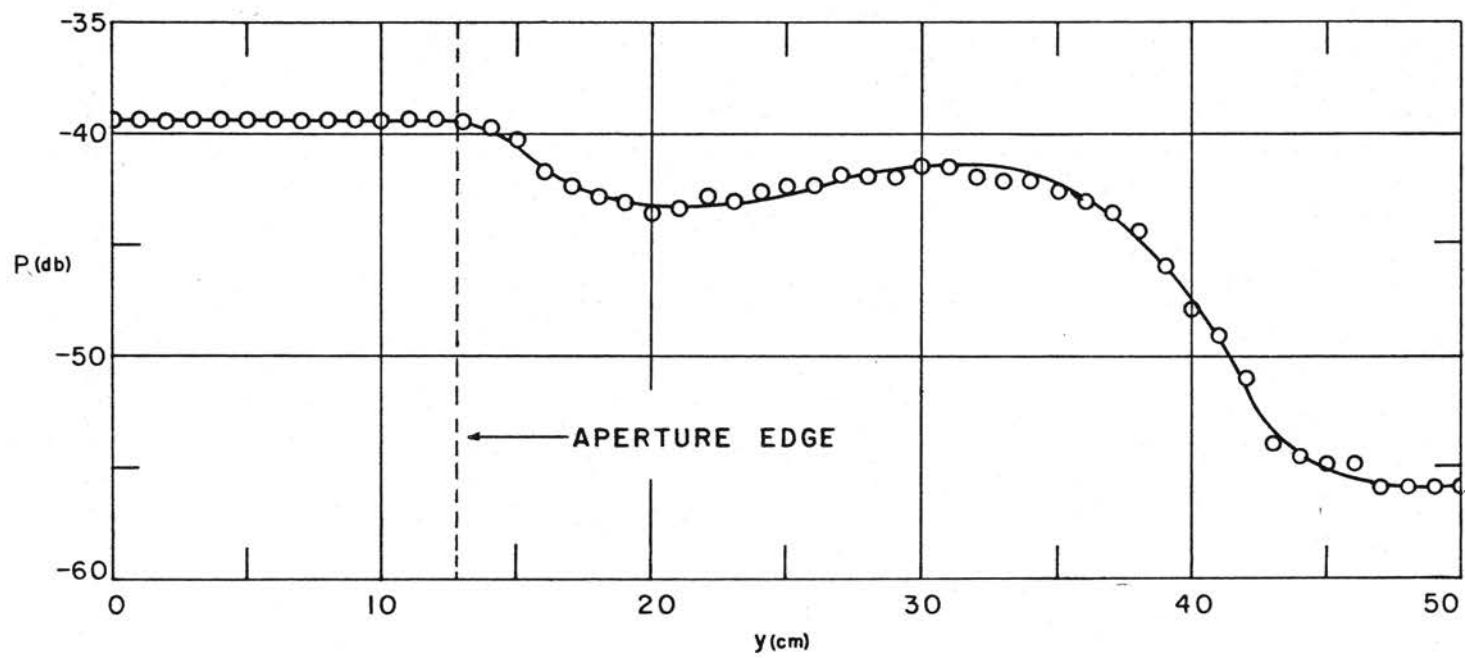
Figure 41. Leakage pressure vs. lateral distance, circular aperture, f = 1500 cps.

APPENDIX II

Because the acoustic output of the horn at constant input voltage and the sensitivity of the microphone with probe cap in place, are not linear functions of frequency a relative comparison of acoustic pressure between the three frequencies is impractical. Thus a separate input voltage was chosen, from response curves, for each frequency such that the amplitude of the wave would be sufficiently large for easy measurements.

From the microphone calibration curves, furnished with the microphone, an approximate pressure level was determined for the $0db$ reference for each of the three frequencies.

Case 1:

The $0db$ reference level for 500 cps. is referred to 100 volts peak to peak output from the hp 450-A amplifier, with an input voltage to the horn of 10 volts peak to peak. From the calibration curves $0db$ corresponds to a pressure of approximately 0.7406 dynes/cm^2.

Case 2:

The $0db$ reference level for 1500 cps. is referred to 100 volts peak to peak from the hp 450-A amplifier, with 15 volts peak to peak input voltage to the horn. From the calibration curves $0db$ corresponds to a pressure of approximately 1.1208 dynes/cm^2.

Case 3:

The $0db$ reference level for 8000 cps. is referred to 100 volts peak to peak output from the hp 450-A amplifier with 50 volts peak to

peak at the input of the horn. Determinations from the calibration curves indicate $0\,db$ corresponds to a pressure of approximately 14.1067 dynes/cm^2.

Comparison of the sensitivities of the two ports on the gradient microphone with the sensitivity of the Kellogg show that at a fixed point in the field the output of either port is $10\,db$ below the output of the Kellogg. Thus the scale of the gradient curves has been shifted to correspond to the calibration of the Kellogg microphone at 1500 cps.

APPENDIX III

The microphone shown in figure 7 was designed to measure the instantaneous pressure difference between the two ports mechanically. Some of the limitations of the microphone which have been found are: (1) the fixed spacing of the two probe tubes puts an upper limit to the useful frequency, (2) interaction between the two probe tubes can distort the field and (3) a mis-match between the two probe tubes and their respective air volumes causes different resonant frequencies between the two sides of the diaphram as well as causing a difference in sensitivity.

Frequency response curves were made with one port closed, on each of the two ports and they show the front port (the port away from pre-amplifier) to be more sensitive than the rear port (the port nearest preamplifier). Also the response curves show the resonant frequencies of the front port to be greater than the resonant frequencies of the rear port. Both conditions were nearly corrected simultaneously by placing two $1\frac{1}{4}$" pieces of bare 18-gage wire in the front port. However, when the axis of the microphone was placed parallel to a plane wave front, that is with $f = 1500$ cps, the output of the microphone was not zero, as it should be if equal pressures are applied to both sides of the membrane. With both tubes closed the output was zero which ruled out possible leakage into the microphone cavities. Further investigation has failed to reveal the cause of this difficulty.

To justify using the gradient microphone for gradient measurements,

the following investigations were made. The effect of reflections from
the preamplifier, supporting rod and flat end of microphone was studied
by making these surfaces essentially non-reflecting by wrapping them
with fiberglass. This proved to have only a slight effect on the out-
put of the microphone.

If the gradient microphone is operating properly, when it is placed
normal to the field of a plane wave, and rotated 90° about a vertical
axis through a point midway between the two ports, the output will
be one-fourth a cycle of a cosine curve. Figure 42 shows a portion of
a cosine curve with the data points as taken from the gradient micro-
phone.

The major deviation of the microphone response from the cosine
curve from 65 to 90 degrees is due to the overriding influence of the
second harmonic. At approximately 65 degrees the second harmonic becomes
significant, and it becomes dominant as the angle of rotation is increased
to 90 degrees. The enhanced response of the gradient microphone to the
second harmonic is possibly due to the geometrical orientation, since
when the relative separation between the supporting rod and the micro-
phone was increased, the second harmonic content of the microphone
output was decreased slightly, but not removed. However, on the basis
of the agreement shown in figure 42, the gradient microphone was used
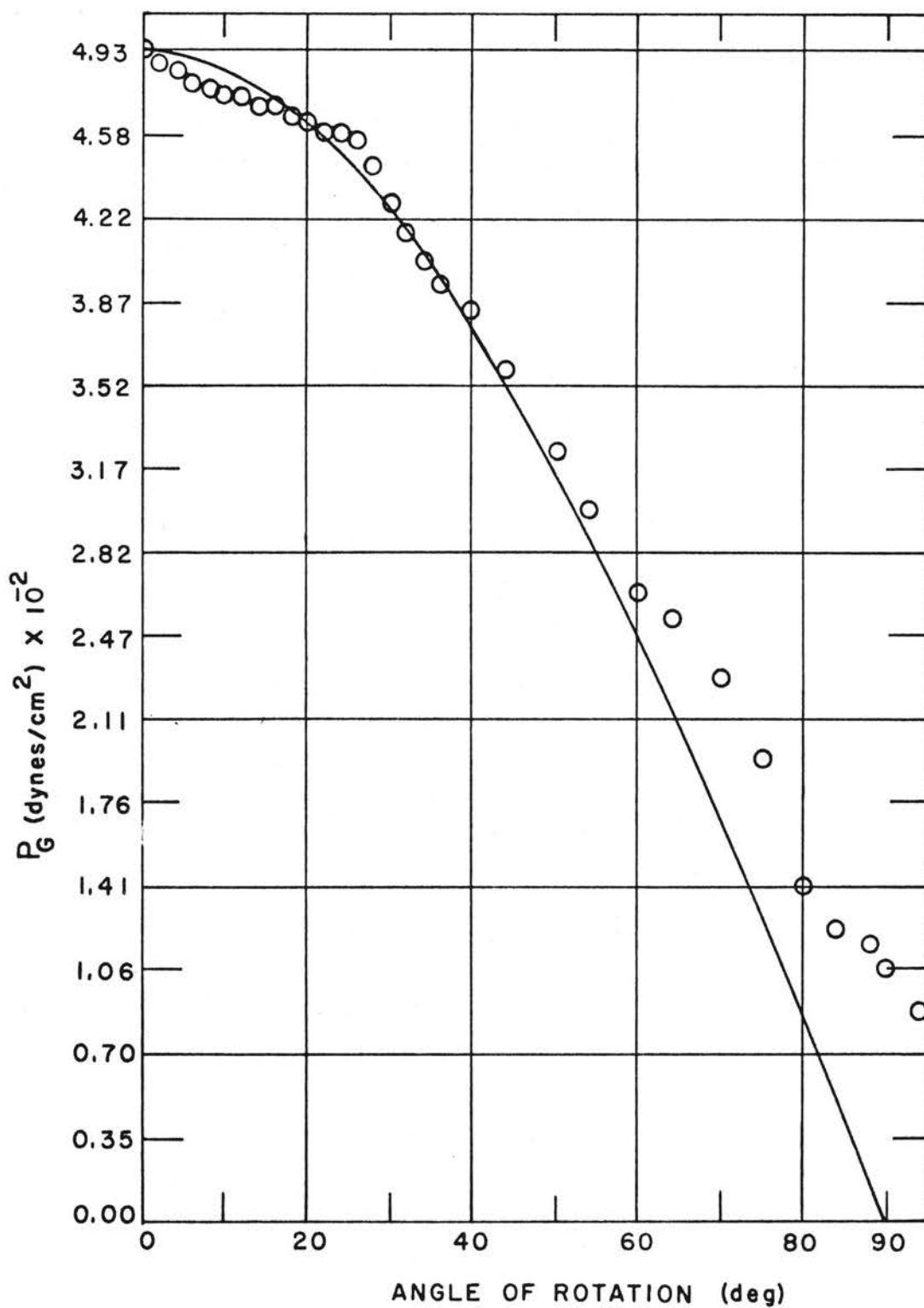for the pressure gradient measurements of Chapter V.

Figure 42. Pressure difference between the two ports of the gradient microphone vs. angle of rotation about an axis at the midpoint of the two ports with microphone in the field of the circular aperture, f = 1500 cps.

VITA

Clifford Wesley Miller, Jr.

Candidate for the Degree of

Master of Science

Thesis: MEASUREMENT OF THE ACOUSTIC FIELD OF RADIATING CIRCULAR AND
RECTANGULAR APERTURES AND A SCATTERING CIRCULAR DISK

Major Field: Physics

Biographical:

Personal Data: Born in Woodward County, Oklahoma, August 7, 1935,
the third child of Clifford W. and A. Mildred Miller.

Education: Attended elementary and high school in Sharon, Oklahoma;
was graduated from Sharon High School in 1952; received the
Bachelor of Science degree from Panhandle Agricultural and
Mechanical College, Goodwell, Oklahoma, in May, 1956; completed
requirements for the Master of Science degree in August, 1961.